EFFECTS OF QUANTUM CONFINEMENT AND COHERENCE IN FINITE-TIME QUANTUM SZILARD ENGINE

by
BEYZA ASLANBAŞ

Submitted to the Graduate School of Engineering and Natural Sciences
in partial fulfilment of
the requirements for the degree of Master of Science

Sabancı University
July 2025

EFFECTS OF QUANTUM CONFINEMENT AND COHERENCE IN FINITE-TIME QUANTUM SZILARD ENGINE

Approved by:

Asst. Prof. ALHUN AYDIN .....
(Thesis Supervisor)

Prof. ÖZGÜR MÜSTECAPLIOĞLU .....

Prof. ZAFER GEDİK .....

Date of Approval: July 18, 2025

ABSTRACT

EFFECTS OF QUANTUM CONFINEMENT AND COHERENCE IN FINITE-TIME QUANTUM SZILARD ENGINE

BEYZA ASLANBAŞ

Physics, M.Sc. Thesis, July 2025

Thesis Supervisor: Asst. Prof. Alhun Aydın

Keywords: finite-time heat engine, information thermodynamics, Landauer principle, open quantum systems

The Szilard engine is a foundational thought experiment that rigorously links thermodynamics and information theory. With the miniaturization of devices and ongoing progress in quantum information science, it is crucial to examine how quantum effects influence the operation of such engines. This thesis investigates the finite-time dynamics of a quantum Szilard engine subjected to size-invariant shape transformations, in which the geometry of the confinement potential is deformed without altering its overall size. The system's evolution is modeled using a time-dependent, Markovian LGKS (Lindblad-Gorini-Kossakowski-Sudarshan) master equation. We numerically solve this equation to analyze the thermodynamic behavior of the engine, focusing on the roles of quantum coherence and its interplay with heat, work, and entropy throughout the cycle. Special attention is given to how coherence evolves under varying barrier insertion rates and thermalization temperatures. We demonstrate that coherence generation is strongly influenced by both the protocol speed and the bath temperature. Furthermore, we show a connection between coherence accumulation and the energetic and informational cost of the cycle. These findings enhance our understanding of coherence in finite-time, measurement-based quantum devices and suggest that geometric deformations can serve as a powerful tool for thermodynamic control in quantum technologies.

ÖZET

SONLU ZAMAN KUANTUM SZILARD ISI MAKİNESİNDE KUANTUM SINIRLAMA VE EŞEVRELİLİĞİN ETKİSİ

BEYZA ASLANBAŞ

Fizik, Yüksek Lisans Tezi, Temmuz 2025

Tez Danışmanı: Dr. Öğr. Üyesi Alhun Aydın

Anahtar Kelimeler: açık kuantum sistemler, bilgi termodinamiği, Landauer ilkesi, sonlu zaman ısı makineleri

Szilard ısı makinesi, termodinamik ve bilgi teorisi arasında bağlantı kuran ünlü bir düşünce deneyidir. Aygıtların küçültülmesi ve bilgi teknolojilerindeki ilerlemelerle birlikte, kuantum mekaniğinin ve kuantum bilgi kuramının Szilard ısı makinesi üzerindeki etkilerini incelemek büyük önem taşımaktadır. Bu çalışma, zamana bağlı Markovian LGKS master denklemi tarafından yönetilen, ölçek değişmez şekil dönüşümleri altında çalışan kuantum Szilard ısı makinesinin sonlu-zamanlı dinamiklerini araştırmaktadır. Bu çalışmada, sistemin ebatlarını değiştirmeden sadece şeklini değiştirerek, termodinamik çevrim sırasında kuantum eşevreliliğin evrimini ve termodinamik etkilerini inceliyoruz. Isı makinesinin sonlu-zamanlı termodinamik analizini master denklemini kullanarak simule ediyoruz. Isı ve iş katkılarından kaynaklanan iç enerji değişimi ve entropi gibi ilgili termodinamik nicelikler de hesaplanmaktadır. Özellikle, farklı bariyer yerleştirme hızları ve termal sıcaklıklar altında eşevreliliğin nasıl davrandığını araştırıyor ve bu sürecin enerjik ve bilgi kuramsal maliyetindeki rolünü inceliyoruz. Ayrıca, sistemde biriken eşevrelilik ile protokolün hızı ve çevrenin sıcaklığı arasında bir bağlantı ortaya koyuyoruz. Bulgularımız, sonlu-zamanlı süreçlerde ve ölçüme dayalı kuantum aygıtlarda eşevreliliğin nasıl üretildiğine dair daha derin bir anlayışa katkıda bulunmakta ve geometrik deformasyonların termodinamik kontrol için potansiyel bir araç olduğunu vurgulamaktadır.

ACKNOWLEDGEMENTS

First, I would like to thank my advisor, Professor Alhun Aydın, for his guidance, support, and encouragement, without applying any pressure. I am also grateful to Dr. Ali Pedram for answering all my questions without judgment and keeping my motivation through insightful and engaging conversations.

I am especially thankful to my dear friends Sevgi Şirin and Ceyda Özer for their comforting friendship and for always being there to listen my existential problems. But most of all, I am deeply thankful to my whole family, to my mother and father, Tülay and Sait, for their endless dedication and hard work for my unending education, and to my sisters Yonca and Eylül for bringing color and joy to my life. As for my little niece and nephew, their cuteness always distracted me from my problems and reminded me what it feels like to be a child again.

Dedicated to
my father

TABLE OF CONTENTS

LIST OF TABLES

LIST OF FIGURES

LIST OF ABBREVIATIONS

CPTP Completely Positive Trace Preserving 12, 20, 22, 24

ICPTP Incoherent Completely Positive Trace Preserving 22

LGKS Lindblad–Gorini–Kossakowski–Sudarshan 9, 23, 35, 39

POVM Positive Operator-Valued Measure ..... viii, 6, 7, 8, 35

SIST Shape Invariant Shape Transformation ..... xi, 28, 30, 42, 49, 53, 55

1. INTRODUCTION

Since the formulation of the second law of thermodynamics in the mid-19th century, its implications have been debated by many scientists (Čápek & Sheehan, 2005). Maxwell's demon thought experiment, which is the most famous objection to the second law of thermodynamics by seemingly indicating the loss of entropy in a closed system, remained paradoxical until the establishment of the connection between information and thermodynamics. In 1929, Leo Szilard revealed the link between information, measurement, and memory by introducing a single particle heat engine invoking Maxwell's demon, which later became known as the Szilard engine (Szilard, 1929). Later, Rolf Landauer discovered that the erasure of information inevitably releases heat, establishing the principle that information is physical (Landauer, 1982). Building upon these, Charles Bennet showed that Maxwell's demon cannot violate the second law of thermodynamics once the thermodynamic cost of erasing the acquired information during measurements, bounded by Landauer's principle (Bennett, 1982).

With the resolution of this fundamental bond between information and thermodynamics together with the development of quantum thermodynamics, the Szilard engine becomes crucial for understanding the behavior of irreversibility and non-equilibrium in finite-time microscopic systems, which cannot be solved by classical thermodynamics. A single particle quasistatic Szilard engine in a quantum domain with quantum measurements has been initially carried out by Zurek, demonstrating the consistency of measurement cost with the second law of thermodynamics (Zurek, 1984). Numerous researchers have been investigated the variants of the quantum Szilard engine (Davies, Thomas & Zahariade, 2021; Kim, Sagawa, De Liberato & Ueda, 2011; Lloyd, 1997).

While these extensions define a limit for work and heat exchanges for several systems, the finite-size and finite-time analysis is essential to capture the quantum effects, such as coherence, size, and shape effects. The validity of Landauer's principle in a quantum Szilard engine considering the finite-size effects in the absence of an explicit Maxwell's demon has been demonstrated (Aydin, Sisman & Kosloff, 2020). They

demonstrate that due to quantum size and shape effects that arise from the quantum confinement in the system, the partition insertion requires work, which is recovered during the expansion. Size-invariant shape transformation, a geometric method that continuously modifies an object's shape while keeping its size constant, allows one to separate the influences of quantum size and shape effects and to examine the pure quantum shape effects in confined systems with quantized energy levels (Aydin, 2023; Aydin & Sisman, 2019),(Aydin & Sisman, 2023).

More recently, a finite-time quantum Szilard engine has been proposed to investigate the trade-off between power and efficiency, using a spin-1/2 particle as a working medium, with Maxwell's demon performing non-ideal quantum measurement to extract work (Zhou, Ma & Sun, 2024). Quantum Szilard engine is also used as an alternative and complementary tool to analyze the extracted work to understand the correlation structure of the system (Brunelli, Genoni, Barbieri & Paternostro, 2017).

Building upon these recent works, here, we investigate the finite-time operation of quantum Szilard engine under size-invariant shape transformations. We argue that the geometric alterations provide a suitable domain for capturing the interplay between coherence, work extraction, and information in finite-size Markovian systems.

In Section 2, we outline the fundamental operations of closed and open system quantum dynamics. Then, we discuss how quantum thermodynamic relations reduce to classical thermodynamics and how the connection between information and thermodynamics is established. Finally, we discuss quantum features such as coherence and the effects of quantum confinement.

In Section 4, we introduce one-dimensional quasistatic Szilard Engine modeled as an n-level system (qudit). We simulate the system in finite-time considering Markovian evolution for various insertion speeds and temperature regimes to understand the trade-off between dissipation and coherence. Additionally, to understand the effect of shape change on coherence in the system, we define a weighted pseudo-coherence measure that focuses on the low-lying energy states of the system.

2. QUANTUM THERMODYNAMICS AND MEASUREMENT

Thermodynamics is the study of energy and energy transformations, which are characterized by work and heat. The dynamical process in classical thermodynamics is insufficient to explain the underlying microscopic evolution of the macroscopic quantities. Unitary and dissipative dynamics of the quantum systems enable a more accurate description of the evolution at small scales where quantum effects and time-dependent behavior become significant. Extending classical thermodynamics to the quantum domain involves including quantum mechanical features, such as coherence, entanglement, and confinement.

This section introduces the closed and open quantum system dynamics and thermodynamic formalism that is used in the thesis. It begins with an overview of the closed, open system dynamics and quantum measurement. Next, the extension of thermodynamic properties to quantum thermodynamics is discussed, emphasizing coherence, the Landauer principle, and finite-time effects. Finally, the geometric implications of quantum thermodynamics due to finite size are explored.

2.1 Closed Quantum System Dynamics

Within the framework of quantum mechanics, the complete description of a system is given by a time-dependent wave function $\psi(t)$ belonging to a Hilbert space $\mathcal{H}$. For an isolated system, its change in time is determined through the Schrödinger equation:

$$i\hbar\frac{d}{dt}|\psi(t)\rangle = H|\psi(t)\rangle, \tag{2.1}$$

where $H(t)$ is Hamiltonian, $\hbar$ is reduced Planck constant. If the system is in an eigenstate of H, it can be written as an eigenvalue equation:

$$H|E_n\rangle = E_n|E_n\rangle. \tag{2.2}$$

where $|E_n\rangle$ denotes eigenstates with energy E_n. Considering $\hbar = 1$ the dynamical solution for $\psi(t)$ can be expressed in terms of unitary time evolution operator $U(t, t_0) = e^{-iH(t-t_0)}$ generated by the system Hamiltonian H with initial condition $U(t_0, t_0) = I$:

$$|\psi(t)\rangle = U(t, t_0)|\psi(t_0)\rangle \tag{2.3}$$

The system's state can also be represented by the density matrix $\rho(t)$:

$$\rho(t) = \sum_i p_i |\psi_i(t)\rangle\langle\psi_i(t)| \tag{2.4}$$

where p_i is the corresponding probability for each state. For pure states ψ, the density matrix is:

$$\rho = |\psi(t)\rangle\langle\psi(t)| \tag{2.5}$$

Although the state vector ψ and density matrix ρ both describe the state of the system, the density operator can also encode incoherent classical mixture of the states. In that case, the density operator takes the following form:

$$\rho = \sum_k p_k |\psi_k\rangle\langle\psi_k| \tag{2.6}$$

where p_k is the probability of being in the state $|\psi_k\rangle$ with the condition $\sum_k p_k = 1$. For pure states, $tr(\rho^2) = 1$ and for mixed states $tr(\rho^2) < 1$.

In the Schrödinger picture, the time evolution of the density operator is

$$\rho(t) = \sum_i p_i U(t, t_0)|\psi_i(t_0)\rangle\langle\psi_i(t_0)|U^\dagger(t, t_0) = U(t, t_0)\rho(t_0)U^\dagger(t, t_0). \tag{2.7}$$

Time derivation of the ρ leads to the Liouville-von Neumann equation equation. The Liouville-von Neumann equation equation describes the time dependence of the density matrix $\rho(t)$,

$$\frac{d}{dt}\rho(t) = -i[H(t), \rho(t)], \tag{2.8}$$

The expectation value of the operator A is given as:

$$\langle A(t)\rangle = \mathrm{tr}(A\rho(t)) \tag{2.9}$$

While in the Schrödinger picture, the time evolution operator acts on states, in Heisenberg's picture, the operators evolve in time

$$A_H(t) = U^\dagger(t,t_0)A(t)U(t,t_0). \tag{2.10}$$

The density matrix is fixed at the initial value as $\rho_H = \rho(t_0)$ because the operators govern time-dependence. Then the equation of motion in the Heisenberg picture is:

$$\frac{d}{dt}A_H(t) = i[H_H(t), A_H(t)] + \left(\frac{\partial A}{\partial t}\right)_H \tag{2.11}$$

where $H_H(t)$ is the time-dependent Hamiltonian in the Heisenberg picture obtained from the Schrödinger picture Hamiltonian $H(t)$,

$$H_H(t) = U^\dagger(t,t_0)H(t)H(t,t_0). \tag{2.12}$$

2.2 Quantum Measurement

Extracting information from a system requires measurement. In contrast to classical measurement, which reveals a definite value without disturbing the system, quantum measurement yields probabilistic outcomes and disturbs the system. Even though the characteristics of quantum measurement raise skepticism about the interpretations of quantum mechanics, for the purpose of this research, I employ the standard interpretation of quantum mechanics to describe the quantum measurement processes.

The quantum state $|\psi\rangle$ is represented as a linear combination of the eigenstates $\{|a_k\rangle\}$ of the operator A:

$$|\psi\rangle = \sum_k c_k|a_k\rangle. \tag{2.13}$$

where $c_k = \langle a_k|\psi\rangle$ are complex coefficients.

Born rule states that measuring an operator A with eigenstates $\{|a_k\rangle\}$ on the state $|\psi\rangle$, the probability of obtaining the state $|a_k\rangle$ yields:

$$P(a_k) = |c_k|^2 = |\langle a_k|\psi\rangle|^2. \tag{2.14}$$

The state collapses to the corresponding eigenstate $|\psi'\rangle = |a_k\rangle$ after the measurement.

Following this principle, projective (Von Neumann) measurement, positive operator valued measurement (POVM), and weak measurements have been introduced to describe different measurement scenarios.

2.2.1 Projective (Von Neumann) Measurements

In the standard formulation of quantum mechanics, a projective measurement is represented by a Hermitian operator A defined on the Hilbert space $\mathcal{H}$. This operator has a spectral decomposition of the form.

$$A = \sum_k a_k \Pi_k, \tag{2.15}$$

where a_k are the real eigenvalues corresponding to possible measurement outcomes, and $\Pi_k = |a_k\rangle\langle a_k|$ are the orthogonal projectors onto the eigenspaces of A. These projectors satisfy the completeness relation $\sum_k \Pi_k = I$ and the orthogonality condition $\Pi_j \Pi_k = \delta_{jk}\Pi_k$.

If the system is in a pure state $|\psi\rangle$, then the probability of the measurement outcome a_k is given by the Born rule:

$$P(a_k) = \langle\psi|\Pi_k|\psi\rangle. \tag{2.16}$$

Following the measurement, the system collapses into the corresponding eigenstate:

$$|\psi'\rangle = \frac{\Pi_k|\psi\rangle}{\sqrt{P(a_k)}} = |a_k\rangle. \tag{2.17}$$

If the system is initially in a mixed state described by a density matrix ρ, then the probability of obtaining the outcome a_k is

$$P(a_k) = \mathrm{tr}[\Pi_k \rho], \tag{2.18}$$

and the post-measurement state becomes

$$\rho' = \frac{\Pi_k \rho \Pi_k}{\mathrm{tr}[\Pi_k \rho]}. \tag{2.19}$$

Projective measurements model the situation in which maximal information is retrieved, and the system collapses fully into one of the eigenstates of the observable in the measurement basis.

The projection $\rho \to \Pi_k \rho \Pi_k$ step is a linear transformation; however, normalization $\mathrm{tr}[\Pi_k \rho]$ causes nonlinearity in the measurement outcome. In classical mechanics also, the measurement induces nonlinearity, yet it does not affect the system's dynamics, only updates the knowledge via Bayes' rule (Jacobs, 2014).

2.2.2 Positive Operator-Valued Measure (POVM)

Positive operator-valued measure (POVM) is a class that a measurement is represented with a set of positive semi-definite operators $\{E_k\}$ acting on the Hilbert space $\mathcal{H}$ such that.

$$\sum_k E_k = I. \tag{2.20}$$

Each operator E_k corresponds to a possible measurement outcome. If the quantum system is in the state ρ, the probability of observing outcome k is given by

$$P(k) = \mathrm{tr}[E_k \rho]. \tag{2.21}$$

The E_k operators are not necessarily orthogonal projectors, and do not, in general, define how the state evolves after the measurement. To describe post-measurement evolution, we introduce a set of Kraus (measurement) operators $\{M_k\}$ such that

$$E_k = M_k^\dagger M_k, \quad \sum_k M_k^\dagger M_k = I. \tag{2.22}$$

Upon observing outcome k, the system is updated according to

$$\rho' = \frac{M_k \rho M_k^\dagger}{\mathrm{tr}[M_k \rho M_k^\dagger]}. \tag{2.23}$$

POVMs generalize projective measurements and allow for descriptions of noisy, weak, or indirect measurements.

2.2.3 Weak Measurements

Unlike projective measurement, POVM description can extract partial information from the system.

Weak measurement was first introduced by Aharonov et. al as a way to probe quantum systems without fully collapsing the state and extracting partial information about an observable through the use of pre- and post-selection(Aharonov, Albert & Vaidman, 1988). While their original formulation introduced the concept of weak values and two-state vector formalism, here we focus on weak measurements as a type of Positive Operator-Valued Measure (POVM) that extracts only a small amount of information about an observable and minimally disturbs the system (Jacobs, 2014).

The total probability of obtaining a result in the range $k \in [a, b]$ using the trace property

$$P(k \in [a,b]) = \sum_{k=a}^{b} \mathrm{tr}\left(M_k \rho M_k^\dagger\right) = \mathrm{tr}\left(\sum_{k=a}^{b} M_k^\dagger M_k \rho\right). \tag{2.24}$$

Then, instead of projecting the system into a single eigenstate, one can express operators that are weighted sums over projectors in Gaussian form, peaked at the eigenstate $|a_k\rangle$, to extract the partial information. These measurement operators are given by

$$M_k = \frac{1}{N} \sum_j e^{-\lambda(a_k - a_j)^2/4} |a_j\rangle\langle a_j|, \tag{2.25}$$

where N is the normalization constant chosen to satisfy the completeness relation $\sum_{k=-\infty}^{\infty} M_k^\dagger M_k = I$.

After the measurement, the final state takes the form

$$\rho_f = \frac{M_k \rho M_k^\dagger}{\mathrm{tr}[M_k \rho M_k^\dagger]} = \frac{1}{N} \sum_j e^{-\lambda(a_j - a_k)^2/2} |a_j\rangle\langle a_j|. \tag{2.26}$$

The final state peaked around eigenvalue λ, with width $1/\sqrt{\lambda}$. When λ is larger, the width is small, resulting in a sharply peaked final state. This corresponds to a

strong measurement. When λ is smaller and the width is larger, the final state is more spread out. This corresponds to a weak measurement with higher uncertainty about the measured value.

2.3 Open Quantum System Dynamics

In realistic physical scenarios, every quantum system interacts with the environment, which influences the system's dynamics and characteristics. The theory of open quantum systems analyzes such systems where the environment induces decoherence, dissipation, and thermalization.

The closed quantum systems evolve unitarily with the Liouville-von Neumann equation (2.8), a special case of the master equation describing the time evolution of the state. In an open quantum system, interaction with the environment leads to non-unitary dynamics of the system's reduced state. While the combined system–environment evolution remains unitary in principle, a full microscopic description is typically infeasible due to the complexity and number of environmental degrees of freedom. Therefore, the reduced dynamics are described using more general formulations such as quantum master equations.

There are various master equations designed for different types of open quantum systems. The Lindblad-Gorini–Kossakowski–Sudarshan (LGKS) master equation formulates the most general class of Markovian dynamics.

In the following, we introduce the formulation of the LGKS master equation using (Breuer & Petruccione, 2002), starting from fundamental assumptions about system-bath coupling and the Markovian approximation, to build a detailed understanding of the following chapters.

If the system interacts with the environment, we can write the total Hamiltonian as follows:

$$H(t) = H_S + H_E + H_I(t) = H_0 + H_I(t) \tag{2.27}$$

H_S, H_E, and H_I are the Hamiltonians of the system, environment, and interaction, respectively. $H_S + H_E = H_0$ represents the free Hamiltonian. The Schrödinger, Heisenberg, and interaction pictures are equivalent representations of unitary quan-

tum dynamics. The interaction (Dirac) picture is particularly useful for perturbative treatments, where the Hamiltonian is split into a solvable part and an interaction term.

The unitary time evolution operator can be separated into free and interaction operators.

$$U(t,t_0) = U_0(t,t_0)U_I(t,t_0) \quad \Rightarrow \quad U_I(t,t_0) = U_0^\dagger(t,t_0)U(t,t_0) \tag{2.28}$$

Using the cyclic property of trace, the expectation value of the operator A in (2.9) can be written in terms of the interaction picture elements:

$$\langle A(t)\rangle = \mathrm{tr}\left(A U_0(t,t_0)U_I(t,t_0)\rho(t_0)U_I^\dagger(t,t_0)U_0^\dagger(t,t_0)\right) = \mathrm{tr}\left(A_I(t)\rho_I(t)\right) \tag{2.29}$$

Where interaction picture operator $A_I(t)$ is

$$A_I(t) = U_0^\dagger(t,t_0)AU_0(t,t_0), \tag{2.30}$$

and state $\rho_I(t)$ in the interaction picture is

$$\rho_I(t) = U_0^\dagger(t,t_0)\rho(t)U_0(t,t_0) = U_I(t,t_0)\rho(t_0)U_I^\dagger(t,t_0). \tag{2.31}$$

The derivative of $\rho_I(t)$ yields the Liouville-von Neumann master equation:

$$\frac{\partial}{\partial t}\rho_I(t) = -i\left[H_I(t),\rho_I(t)\right], \tag{2.32}$$

Taking the integral of both sides results in:

$$\rho_I(t) = \rho_I(t_0) - i\int_{t_0}^{t} ds\,\left[H_I(s),\rho_I(s)\right] \tag{2.33}$$

We trace the environment to determine the system's evolution during the interaction.

$$\frac{\partial}{\partial t}\rho_{IS}(t) = -i\,\mathrm{tr}_E\left[H_I(t),\rho_I(t_0)\right] - \int_0^t ds\,\mathrm{tr}_E\left[H_I(t),[H_I(s),\rho_I(s)]\right] \tag{2.34}$$

Where ρ_{IS} is the reduced density operator of the system in the interaction picture.

We now consider that the environment and the system do not correlate at the initial time $t = t_0$. The initial density operator then takes the following form:

$$\rho_I(t_0) = \rho_S(t_0) \otimes \rho_E(t_0) \tag{2.35}$$

In the case of correlation between the system and the environment, the time evolution of the interaction state for $t > t_0$ becomes

$$\rho_I(t) \neq \rho_s(t) \otimes \rho_E(t). \tag{2.36}$$

In weak coupling regimes, the environment is much larger than the system, so the state of the environment is not affected by the system. Born approximations assumes that $\rho_E(t_0) = \rho_E$ for all times. Hence, the time evolution of the interaction state becomes:

$$\rho_I(t) \approx \rho_{IS}(t) \otimes \rho_E \tag{2.37}$$

ρ_{IS} is defined by tracing out the environment. The final form of the equation Eq. 2.34 is as follows:

$$\frac{\partial \rho_{IS}(t)}{\partial t} = -\int_0^t ds \, \mathrm{tr}_E \left[H_I(t), [H_I(s), \rho_{IS}(s) \otimes \rho_E] \right] \tag{2.38}$$

As time evolves, the interaction between the system and environment generally induces correlations, making the total density matrix ρ_I entangled and no longer separable. To prevent such correlation, Markov approximation is applied in which the environment is considered "memoryless" so that it forgets any information about the system. The integral of $[H_I(t), \rho_{IS}(t)]$ represents the evolution of the density matrix of the system due to interaction with the environment at previous times; that time s influences from 0 to the current time t. In cases where the time of the memory of environmental interaction is considerably shorter in comparison to the system evolution time, then we can apply Markovian approximation as $\rho_{IS}(s) \to \rho_{IS}(t)$.

$$\frac{d}{dt}\rho_{IS}(t) = -\int_0^t ds \, \mathrm{tr}_E \left[H_I(t), [H_I(s), \rho_{IS}(t) \otimes \rho_E] \right]. \tag{2.39}$$

The equation Eq. 2.39 is referred to as the Redfield equation, which is local in time. The time evolution of the density operator is still dependent on the initial time $t_0 = 0$, which implies that time evolution is influenced by memory. To derive a memoryless

(Markovian) master equation, one typically starts from the Redfield equation and imposes additional approximations—such as the secular approximation—to cast it into the Lindblad form, which generates a quantum dynamical semigroup. A semigroup description of the system's dynamics is valid when the environment has a short correlation time, ensuring that memory effects are negligible. For completely positive, trace preserving (CPTP) quantum dynamical system $\mathrm{tr}_S\{V(t)\rho_S\} = \mathrm{tr}_S\rho_S = 1$ time evolution operator $V(t)$ obey the semigroup property:

$$T(t+s) = T(t)T(s), \text{ for all } t, s \geq 0. \tag{2.40}$$

Based on Eq. 2.40, the evolution operator $V(t)$ can be separated into sequences. If we substitute $s \to t - s$, the terms in the integral can be stated in terms of the current time and previous time. This substitution reflects the memory effects of the correlation between the system and the environment. On the other hand, the semigroup property implies that system time evolution only depends on the current state and time. Likewise, because $s \gg t - s$, we can conclude that the time scale of the system s is much larger than the time scale of the evolution of the correlation $t - s$. Therefore, the bounds of the integral can be replaced by infinity. Thus, in the case of a weak correlation between the system and environment, the Markovian master equation takes the following form in the interaction picture:

$$\frac{d}{dt}\rho_{IS}(t) = -\int_0^\infty ds\, \mathrm{tr}_E\left[H_I(t), [H_I(t-s), \rho_{IS}(t) \otimes \rho_E]\right]. \tag{2.41}$$

Now, we can dive into explaining the terms and the correlation to proceed towards the Lindblad form.In the interaction picture, the interaction Hamiltonian $H_I(t)$ can be break down into the system part $A_\alpha(t) = e^{iH_S t} A_\alpha e^{-iH_S t}$ and the environment part $B_\alpha = e^{iH_E t} B_\alpha e^{-iH_E t}$, as given below:

$$H_I(t) = \sum_\alpha A_\alpha(t) \otimes B_\alpha(t) \tag{2.42}$$

The environment correlation function interprets the dependence of environmental fluctuations at different times. It is defined as follows:

$$C_{\alpha\beta}(t,s) = \langle B_\alpha(t) B_\beta(s) \rangle_E = \mathrm{tr}_E\left(B_\alpha(t) B_\beta(s) \rho_E\right). \tag{2.43}$$

Because environment is stationary $[H_E, \rho_E] = 0$. Time translation of the correlation function:

$$\langle B_\alpha(t+\tau)B_\beta(s+\tau)\rangle_E = \langle B_\alpha(t)B_\beta(s)\rangle_E \tag{2.44}$$

If we replace $\tau = -s$:

$$\langle B_\alpha(t-s)B_\beta(0)\rangle_E = \langle B_\alpha(t)B_\beta(s)\rangle_E \tag{2.45}$$

This means that the correlation only depends on the time difference t-s. So $C_{\alpha\beta}(t,s) = C_{\alpha\beta}(t-s)$ Embedding Eq. 2.42 and the description of the correlation function, the master equation Eq. 2.41 takes the following form:

$$\frac{\partial \rho_{IS}(t)}{\partial t} = -\sum_{\alpha\beta}\int_0^\infty d\tau \left([A_\alpha(t), A_\beta(t-\tau)\rho_{IS}(t)]C_{\alpha\beta}(\tau) + [\rho_{IS}(t)A_\beta(t-\tau), A_\alpha(t)]C_{\beta\alpha}(-\tau)\right). \tag{2.46}$$

Converting Eq. 2.46 into the Schrödinger picture Eq. 2.7 using the transformation between Schrödinger and interaction pictures:

$$\rho_{IS}(t) = e^{iH_S t}\rho_S(t)e^{-iH_S t} \qquad\qquad \rho_S(t) = e^{-iH_S t}\rho_{IS}(t)e^{iH_S t} \tag{2.47}$$

$$\frac{\partial \rho_S(t)}{\partial t} = -i[H_S, \rho_S(t)] + e^{-iH_S t}\frac{\partial \rho_{IS}(t)}{\partial t}e^{iH_S t} \tag{2.48}$$

Then, the final form of the master equation is as follows:

$$\frac{d}{dt}\rho_S(t) = -i[H_S, \rho_S(t)] - \sum_{\alpha\beta}\int_0^\infty d\tau \left([A_\alpha, A_\beta(-\tau)\rho_S(t)]C_{\alpha\beta}(\tau) + [\rho_S(t)A_\beta(-\tau), A_\alpha]C_{\beta\alpha}(-\tau)\right) \tag{2.49}$$

The system operators $A_\alpha(t)$ oscillate in time due to the system Hamiltonian H_S. We can decompose them into components that rotate at specific frequencies ω, similar to breaking a musical chord into individual notes:

$$A_\alpha(t) = \sum_\omega e^{-i\omega t}A_\alpha(\omega) \tag{2.50}$$

Each $A_\alpha(\omega)$ is like a "note" that changes the system's energy by ω. $[H_S, A_\alpha(\omega)] = -\omega A_\alpha(\omega)$ means that $A_\alpha(\omega)$ reduces the system's energy by ω when $\omega > 0$. When we plug this decomposition into the master equation, we get terms like:

$$e^{-i(\omega+\omega')t} A_\alpha(\omega) A_\beta(\omega') \rho(t) \tag{2.51}$$

Terms with $\omega \neq -\omega'$ oscillate rapidly and average to zero over time, much like high-pitched noise that can be ignored. In contrast, terms with $\omega = -\omega'$ vary slowly or remain constant, so they survive in the long-time dynamics. This is analogous to tuning a radio: we keep only the clear station (resonant terms) and ignore the static (fast oscillations).

The remaining time integral takes the form:

$$\int_0^\infty d\tau \, C_{\alpha\beta}(\tau) e^{i\omega\tau} \equiv \Gamma_{\alpha\beta}(\omega), \tag{2.52}$$

where $\Gamma_{\alpha\beta}(\omega)$ is the one-sided Fourier transform of the environment correlation function $C_{\alpha\beta}(\tau)$. This quantity is a complex, time-independent rate. Its real part, denoted $\gamma_{\alpha\beta}(\omega)$, determines the dissipation rates, while the imaginary part contributes to a correction of the system Hamiltonian known as the Lamb shift, denoted H_{LS} which is often omitted in the evolution of the heat engines because it does not contribute directly to dissipation or heat exchange.

Combining all these results, the master equation finally takes the Lindblad form:

$$\dot{\rho}_S(t) = -i[H_S + H_{LS}, \rho_S(t)] + \sum_{\omega,\alpha,\beta} \gamma_{\alpha\beta}(\omega) \left(A_\beta(\omega) \rho_S(t) A_\alpha^\dagger(\omega) - \frac{1}{2} \{ A_\alpha^\dagger(\omega) A_\beta(\omega), \rho_S(t) \} \right), \tag{2.53}$$

which ensures complete positivity and trace preservation. This form is generally used to model the reduced dynamics of open quantum systems in the weak-coupling, Markovian limit.

2.4 Quantum Thermodynamics

Quantum mechanics provides the fundamental framework for describing the dynamics of small systems such as atoms and particles. In contrast, thermodynamics governs the statistical behavior of large ensembles of particles. The main challenge is to understand how thermodynamics concepts and laws such as temperature, entropy, and the second-law emerges from the quantum properties of a few or many particles. The goal of quantum thermodynamics is to develop microscopic models

that explain the emergence of thermodynamic behavior from quantum principles (Vinjanampathy & Anders, 2016).

This section offers a summary of fundamental principles in quantum thermodynamics based on the comprehensive reviews Vinjanampathy & Anders (2016), Kosloff (2013). Starting from the role of information in the thermodynamic process, a discussion on information and thermodynamics is introduced.

2.4.1 Classical to Quantum Thermodynamics

The zeroth law of thermodynamics defines the temperature and separates the definition of the system and bath by stating that if A is in thermal equilibrium with B, and B is in equilibrium with another system C, then A and C are also in equilibrium. This relation makes the temperature a meaningful and measurable property. The first law expresses energy conservation by relating change in system internal energy U to heat added Q and work W done by the system through equation $\Delta U = Q + W$. The second law states that the entropy of an isolated system cannot decrease ($\Delta S \geq 0$), which leads to the irreversibility and breakdown of the time-reversal symmetry. The third law asserts that absolute zero temperature cannot be reached in a finite number of steps.

In classical thermodynamics, internal energy is the average total Hamiltonian of the system. The same definition also holds for quantum systems. For quantum system in state ρ and Hamiltonian H, internal energy is:

$$U(\rho) = \sum_i p_i E_i = \mathrm{tr}(\rho H). \tag{2.54}$$

The change in internal energy is

$$\Delta U = U(\tau) - U(0) = \int_0^\tau \frac{dU}{dt} dt = \int_0^\tau \mathrm{tr}\left[\dot{\rho}(t) H(t)\right] dt + \int_0^\tau \mathrm{tr}\left[\rho(t) \dot{H}(t)\right] dt \tag{2.55}$$

Then defining average heat absorbed by the system and the average work done on the system as follows corresponds Eq. 2.55 to the first law of thermodynamics.

$$\langle Q \rangle = \int_0^\tau \mathrm{tr}[\dot{\rho}(t) H(t)]\, dt, \quad \langle W \rangle = \int_0^\tau \mathrm{tr}[\rho(t) \dot{H}(t)]\, dt \tag{2.56}$$

Work is extracted from the system when $\langle W_{ext} \rangle = -\langle W \rangle > 0$, heat is dissipated from the system to the environment when $\langle Q_{dis} \rangle = -\langle Q \rangle > 0$.

$$\langle Q \rangle + \langle W \rangle = \int_0^\tau \frac{d}{dt} \mathrm{tr}\left[\rho(t)H(t)\right] dt = \mathrm{tr}\left[\rho(\tau)H(\tau)\right] - \mathrm{tr}\left[\rho(0)H(0)\right] = \Delta U \quad (2.57)$$

Carnot finds that the maximum efficiency of heat engines operating between hot T_H and cold T_C temperatures is $\eta = 1 - \frac{T_C}{T_H}$. Later, Clausius discovered that less efficiency than the Carnot efficiency is caused by irreversibility and generalized it in the Clausius inequality $\oint \frac{\delta Q}{T} \leq 0$, which quantifies the deviation from the reversibility. The state function entropy as:

$$\Delta S \geq \int \frac{\delta Q}{T} \quad (2.58)$$

Even though Clausius's formula defines the entropy change, it does not explicitly specify the absolute value of entropy. While Boltzmann is trying to understand how systems evolve toward equilibrium, he established the relation between macroscopic quantities like energy, pressure, and volume and microscopic quantities like position and momentum. Then, he discovered that the number of available microstates is connected to entropy and the maximum possible microstate (Boltzmann distribution) corresponds to equilibrium.(Boltzmann, 1877) Later, with the contribution of Max Planck (Planck, 1978), the Boltzmann entropy is formulated as:

$$S = k_B \ln \Omega \quad (2.59)$$

where k_B is the Boltzmann constant and Ω is the number of available microstates. The change is Boltzmann entropy also salsifies the Clausius inequality.

Then Gibbs extended the concept of entropy accounting the probability of each microstate (Gibbs, 1878)

$$S = -k_B \sum_i p_i \ln p_i \quad (2.60)$$

where $p_i = 1/\Omega$ is the probability of the system being in microstate i.

In his foundational work, John Von Neumann (Von Neumann, 2013) introduced the density matrix formalism Eq. 2.6 to describe quantum states. Then he extended the Gibbs entropy to quantum domain. In his work, the entropy in quantum description is expressed as:

$$S(\rho) = -k_B \,\mathrm{tr}[\rho \ln \rho]. \quad (2.61)$$

For thermal thermal equilibrium states where $\rho_{th} = e^{-\beta H}/Z$ von Neumann entropy $S(\rho_{th})$ exactly matches the Gibbs entropy. However, for non-thermal states, this equivalence becomes less straightforward and raises some debates in quantum thermodynamics. Although some non-equilibrium resources depend on coherence and correlation, the von Neumann entropy does not capture those effects. So, alternative coherence and correlation measures are used. Despite these concerns, the suitability of von Neumann entropy as a quantum thermodynamic entropy has been supported by many works, including the Landauer principle. In this thesis, the Von Neumann entropy is used as the general quantum thermodynamical entropy.

The relation between classical and quantum thermodynamics heat, work and entropy implies that we can extend the fundamental thermodynamic relations to quantum thermodynamics. Eq. 2.58 shows that The system's heat intake is restricted by the change in entropy as $Q \geq T\Delta S$. Using this, the free energy, amount of extractable work at constant temperature and volume, is defined as:

$$F(\rho) = U(\rho) - TS(\rho) \tag{2.62}$$

This free energy also sets the upper limit on the work extracted from the system in equilibrium

$$\langle W_{\text{ext}} \rangle = -\langle W \rangle = -\Delta U + \langle Q \rangle \geq -\Delta U + T\Delta S_{\text{th}} = -\Delta F. \tag{2.63}$$

2.4.2 Information and Thermodynamics

In 1948 Claude Shannon made the analog of thermodynamics entropy which is known as information entropy (Shannon, 1948). He quantified the entropy as mathematical formalism of lost information:

$$H = -K \sum_{i=1}^{n} p_i \log p_i \tag{2.64}$$

where K is scaling factor ($K = k_B$ in thermodynamics). Even though the similarity between information entropy and thermodynamics entropy seems obvious, up until the development of Landauer's principle and the study of Maxwell's demon, the physical connection between information and thermodynamics was not understood.

In 1867, James Clerk Maxwell proposed a thought experiment known as Maxwell's Demon. This thought experiment consists a box filled with gas, divided with a partition in the middle. The demon separates the hot gas molecules to the left and cold gas molecules to the right. In the end, all the gas molecules are separated by their temperatures causing the entropy of the system is reduced. Which seemingly breaks the second law of thermodynamics.

In 1929, Leo Szilard formulated an engine which is thermodynamical analog of Maxwell's demon thought experiment (Szilard, 1929). The classical version of the Szilard Engine consists of a single particle in a box with volume V_0, which goes through four steps in isothermal conditions.

First, a box with a single particle inside is divided into two equal parts with the quasistatic insertion of a partition. No work or heat is extracted or done on the system. As a result, no entropy change occurs, the system always remains in equilibrium. After the partition is added to the system, we have no information regarding which side of the box the particle is located. The demon applies a measurement to learn the location of the particle, right or left. Again, during the measurement process, no work or heat exchange occurs between the system and the heat bath, and the system's entropy remains the same. According to the measurement result, the partition starts to move on the opposite side where the particle is located. When the partition reaches the end of the wall, the expansion stops, and work can be extracted. For ideal gas, the extracted work is calculated as:

$$W = \int_V^{V/2} P\,dV = k_B T \int_V^{V/2} \frac{dV}{V} = k_B T \ln 2 \tag{2.65}$$

The heat transfer occurs from the heat bath to the system. In thermodynamics, the system's total energy is $\Delta U = W + Q$, which is equal to $U = W + TS$. In the isothermal compression process, the system's internal energy does not change $\delta U = 0$, so $\Delta W = -T\Delta S$. From here, the entropy change of the system is $\Delta S = -k_B \ln 2$. Extraction of work results in heat being lost in the system in the same amount. Then the partition leaves the box without causing any work and heat exchange.

The decrease of entropy by $\Delta S = -k_B \ln 2$ seemingly violates the second law of thermodynamics, which states that entropy either increases or stays constant.

In 1961, Rolf Landauer showed the relation between entropy and information (Landauer, 1982). The information erasure is a logically irreversible operation where a bit, initially in an unknown state (0 or 1), is reset to a definite state (say, 0). Landauer modeled the bit as a physical system with two distinct states represented

by two separate regions in phase space. Erasing a bit corresponds to decreasing the phase space volume from two possible states into one, reducing the system's entropy by $S = k_B \ln 2$.

According to the second law of thermodynamics, total entropy cannot decrease. Therefore, this reduction in system entropy must be compensated by an equal or greater increase in the environment's entropy (Sagawa, 2012a). Landauer showed that erasing one bit of information causes heat dissipation as

$$\langle Q_{dis}^{min} \rangle = k_B T \ln 2. \tag{2.66}$$

In a more general sense, the Landauer principle asserts that the heat Q released to the surroundings during the erasure of information cannot be less than the corresponding change in the memory's entropy ΔS.

$$Q \geq T\Delta S \tag{2.67}$$

Later, in 1982, Charles Bennet used Landauer's principle to solve Maxwell's demon paradox (Bennett, 1982). The measurement information causes the decrease of the entropy. The measurement device, like Demon, stores one bit of information about the particle's location, which is equal to Shannon entropy $S = -k_B \ln 2$. After the expansion systems return to the initial state and the demon no longer knows the particle's location, information is erased, and $k_B T \ln 2$ heat is dissipated to the environment. Extracted work turns into heat. While these arguments are originally made for classical information, they have since been extended to apply to the information erasure of quantum states ρ.

The progression, from Carnot to Bennet, reveals the fundamental connection between thermodynamics and information theory.

2.4.3 Coherence

Quantum coherence is a fundamental feature of quantum systems arising from the presence of superposition, and it manifests as interference between quantum states. It reflects the existence of well-defined phase relations between different basis states and plays a central role in distinguishing quantum from classical behavior. The off-

diagonal elements of density matrix $\rho_{ij} = \langle i|\rho|j\rangle$ where $i \neq j$ represent the coherence terms.

Coherence measures are used to quantify the degree of superposition in a system relative to a chosen basis. To properly define such measures, we must first establish what constitutes an incoherent state and operation (Baumgratz, Cramer & Plenio, 2014). The incoherent states are the diagonal element of the density matrix shown as:

$$\rho_{incoh} = \sum_i p_i |i\rangle\langle i| \in \mathcal{I}. \tag{2.68}$$

Selective and non-selective incoherent operations form the minimal complete set that captures all possible incoherent state transformations and measurement scenarios (Yadin, Ma, Girolami, Gu & Vedral, 2016). Therefore, considering both types of operations is sufficient to fully describe the effects of coherence in quantum thermodynamic processes.

The properties of incoherent operations, originally formulated in (Baumgratz et al., 2014), are reviewed here, and their proofs are included for clarity and completeness.

Statement 1. A non-selective incoherent CPTP quantum operation ϕ, which consists of a set of incoherent Kraus operators M_k, does not generate coherence. It's action on a state is given by:

$$\Phi(\rho) = \sum_k M_k \rho M_k^\dagger, \quad \sum_k M_k^\dagger M_k = I. \tag{2.69}$$

Proof. Extending the initial state ρ_{incoh} gives:

$$\Phi(\rho) = \sum_k M_k \rho M_k^\dagger = \sum_k M_k \left(\sum_i p_i \, |i\rangle\langle i| \right) M_k^\dagger = \sum_{k,i} p_i \, M_k |i\rangle\langle i| M_k^\dagger. \tag{2.70}$$

Since each M_k is incoherent, $M_k|i\rangle$ maps the state into a basis state with single component $|f_k(i)\rangle$, where f_k is an index function. Thus:

$$M_k |i\rangle\langle i| M_k^\dagger = q_{k,i} |f_k(i)\rangle\langle f_k(i)| \quad (q_{k,i} \geq 0) \tag{2.71}$$

Substituting back to $\phi(\rho)$:

$$\Phi(\rho) = \sum_{k,i} p_i q_{k,i} |f_k(i)\rangle\langle f_k(i)| = \sum_j \left(\sum_{k,i \;\; f_k(i)=j} p_i q_{k,i} \right) |j\rangle\langle j|, \tag{2.72}$$

which remains diagonal in the basis $|j\rangle$.

For the case where initial state ρ has coherence term between basis$\{|k\rangle\}$ and $\{|l\rangle\}$ after the application of projection operator which is described by a quantum map $\Pi(\rho) = \sum_i \Pi_i \rho \Pi_i$, these coherent terms destroyed. We can prove this by checking the amplitude after the projection:

$$\langle k|\Pi(\rho)|l\rangle = \langle k| \left(\sum_i \Pi_i \rho \Pi_i \right) |l\rangle = \sum_i \langle k|\Pi_i \rho \Pi_i|l\rangle \tag{2.73}$$

The off-diagonal terms ($k \neq l$) become:

$$\langle k|\Pi_i \rho \Pi_i|l\rangle = \langle k|i\rangle\langle i|\rho|i\rangle\langle i|l\rangle = \delta_{ki}\delta_{il}\langle i|\rho|i\rangle = 0 \tag{2.74}$$

The final state has only diagonal terms:

$$\rho \to \rho' = \sum_i \langle i|\rho|i\rangle |i\rangle\langle i| \tag{2.75}$$

All coherence terms vanish, and the final state is diagonal. This proves that the coherence cannot increase by the ICTP operations.

Statement 2. The selective incoherent quantum operations applied to incoherent state ($M_k \mathcal{I} M_k^\dagger \subseteq \mathcal{I}$) can not not produce coherence.

Proof. The post measurement state when selective quantum operation applied to incoherent state is:

$$\rho_k = \frac{M_k \rho M_k^\dagger}{p_k}, \quad p_k = \mathrm{tr}[M_k \rho M_k^\dagger]. \tag{2.76}$$

The numerator is the same operation as in Statement 1. The denominator $p_n = \mathrm{tr}[M_n \rho M_n^\dagger]$ normalization which does not effects the coherent terms. As a result selective measurement also keeps the incoherence.

If we apply the the same operation of coherent state the coherence are destroyed.

After introducing a class of incoherent operations that do not generate coherence and preserve the set of incoherent states, we can differentiate a broader class of quantum operations that create or destroy coherence. Coherent operations are operations outside the class of incoherent operations, which are any quantum operation that

transforms an incoherent state into a coherent one. Mathematically if any Kraus operator M_k in a quantum operation $\Phi(\rho) = \sum_k M_k \rho M_k^\dagger$ maps at least one basis state to a superposition such as $M_k|I\rangle$ is non-classical for some $|I\rangle$), then Φ is definitely coherent.

Based on these properties of incoherent and coherent operations, the corresponding requirements for coherence measures are (Baumgratz et al., 2014):

1.1 **Non-negativity**
Rule: $C(\rho) \geq 0$ for all density matrices ρ.
Reason: Coherence quantifies the degree of quantumness or deviation from classical behavior in a state.

1.2 **Monotonicity under ICPTP maps**
Rule: $C(\mathcal{E}(\rho)) \leq C(\rho)$ for any incoherent completely positive trace-preserving (CPTP) map $\mathcal{E}$.
Reason: CPTP maps, such as non-selective measurement, do not increase coherent terms.

1.3 **Monotonicity under selective measurements**
Rule: $\sum_m p_m C(\rho_m) \leq C(\rho)$, where $\rho_m = \frac{M_m \rho M_m^\dagger}{p_m}$ are the post-measurement states and $p_m = \mathrm{tr}(M_m \rho M_m^\dagger)$ is the probability of outcome m.
Reason: This ensures that when post-measurement states are selected, the coherence do not increase.

1.4 **Convexity**
Rule: $C\left(\sum_i p_i \rho_i\right) \leq \sum_i p_i C(\rho_i)$ for any mixed state $\rho = \sum_i p_i \rho_i$.
Reason: Convex mixing of states does not increase average coherence.

The most commonly used coherence measures, l_1 norm and the relative entropy, satisfy all the above conditions. Both are based on distance measures. l_1 norm quantifies coherence as the sum of the absolute values of the off-diagonal elements of the density matrix,which is defined as:

$$C_{l_1}(\rho) = \sum_{i \neq j} |\rho_{i,j}|, \tag{2.77}$$

$$C_{\text{rel.ent.}}(\rho) = S(\rho_{\text{diag}}) - S(\rho), \tag{2.78}$$

where $S(\rho) = -\mathrm{tr}(\rho \log \rho)$ is the von Neumann entropy and ρ_{diag} is the state obtained by discarding all off-diagonal elements of ρ. The relative entropy of coherence mea-

sures quantifies the distance between a quantum state and its closest incoherent state using the quantum relative entropy.

Coherence plays an important role in the thermodynamics behaviors. Coherence can be used as a resource to extract work. When a quantum system initially in a coherent state ρ is projected onto a basis through a decohering operation ,the process removes coherence and increases the system's entropy. It has been demonstrated that work can be obtained from the initial state coherence with a projection process (Kammerlander & Anders, 2016). For example, when the projection is performed in the energy basis $\{|k\rangle\}$ of a Hamiltonian $H = \sum_k E_k |k\rangle\langle k|$ with eigenenergies E_k, the maximum average work that can be extracted. If we compare the initial entropy defined as $S(\rho) = -\operatorname{tr}(\rho \ln \rho)$ with entropy after projection $S(\Pi(\rho)) = -\operatorname{tr}(\Pi(\rho) \ln \Pi(\rho))$, the decrease in entropy can be harnessed to extract work:

$$\langle W_{\max} \rangle = k_B T \left[S\left(\Pi(\rho)\right) - S(\rho) \right] \tag{2.79}$$

The proof of entropy decrease resulting from the projection is demonstrated in (Gemmer & Anders, 2015).

2.4.4 Finite-Time Landauer Principle

The Landauer bound Eq. 2.66 is holds in quasistatic limit, where the system evolve infinitely slowly. However, in realistic scenarios, information erasure occurs much faster. Hence, generalizing the Landauer principle to finite-time processes is necessary for understanding the resulting dissipation.

In the Markovian regime where system is governed by the LGKS master equation Eq. 3.4, for arbitrary driving protocols, correction term to Landauer bound is shown by Van Vu & Saito (2022).

the entropy difference between initial state ρ_0 and the state at τ is:

$$\Delta S = \operatorname{tr}(\rho_\tau \ln \rho_\tau) - \operatorname{tr}(\rho_0 \ln \rho_0) \tag{2.80}$$

And the heat is:

$$Q = -\int_0^\tau \operatorname{tr}(H_t \dot{\rho}_t) dt \tag{2.81}$$

So using the Landauer bound Eq. 2.66, the irreversible entropy production can be written as $\Sigma_\tau = -\Delta S + \beta Q \geq 0$. In the case of appearance of finite-time effects addition irreversible entropy is produced. Adding the correction terms gives:

$$\beta Q \geq \Delta S + \frac{\|\rho_0 - \rho_\tau\|_1^2}{2\tau\bar{\gamma}_\tau} \geq \Delta S + \frac{[2(1-1/d) - \varepsilon]^2}{2\tau\bar{\gamma}_\tau}. \tag{2.82}$$

where $\|\rho_0 - \rho_\tau\|_1$ denotes the trace distance between the initial and final states, and $\epsilon = \|\rho_\tau - |0\rangle\langle 0|\|_1$ measures the deviation from the ground state. The quantity $\bar{\gamma}$ is the time-averaged dynamical activity, characterizing the thermal relaxation timescale, and is defined as $\bar{\gamma} = \tau^{-1}\int_0^\tau \sum_k \mathrm{tr}\left[L_k(t)\rho_t L_k(t)^\dagger\right] dt$ (Van Vu & Saito, 2022). This relation indicates that erasing information over a finite time requires an additional dissipative cost, which is inversely related to both the system's driving speed and its closeness to the target state.

The effect of coherence lay in the difference between initial state ρ_0 and the target state ρ_τ. Dephasing map $\Lambda(\rho) = \sum_n \Pi_n \rho \Pi_n$ where Π_n project the state into nth instantaneous eigenstate of system's Hamiltonian $H(\tau)$, removes the coherence terms, and leaves only diagonal terms which corresponds to classical terms Eq. 2.75. Using the trace norm contractivity property of the CPTP maps diagonal terms and coherence terms C_{res} can be separated as:

$$\|\rho_0 - \rho_\tau\|_1 = \|\Lambda(\rho_0) - \Lambda(\rho_\tau)\|_1 + C_{\mathrm{res}}, \tag{2.83}$$

If we separate the entropy production into diagonal (classical) contribution $\Delta S_{\mathrm{cl}} = S(\Lambda(\rho_0)) - S(\Lambda(\rho_\tau))$ and the entropy caused by coherence, given by the relative entropy of coherence $C_{\mathrm{rel}} = S(\Lambda(\rho_\tau)\|\rho_\tau) = S(\Lambda(\rho_\tau)) - S(\rho_\tau)$ then it becomes:

$$\Delta S = \Delta S_{cl} + C_{rel} \tag{2.84}$$

The lower bound Eq. 2.82 can be further written as:

$$\beta Q \geq \Delta S_{\mathrm{cl}} + \frac{\|\Lambda(\rho_0) - \Lambda(\rho_\tau)\|_1^2}{2\tau\bar{\gamma}_\tau} + C_{\mathrm{rel}} + \frac{C_{\mathrm{res}}}{2\tau\bar{\gamma}_\tau} \tag{2.85}$$

While this equation captures the left over coherence in the final state, the dynamically generated coherence during the erasure is not accounted. If the coherence is quantified with the l_1 norm coherence measure Eq 2.77, the amount of coherence in time τ is:

$$C_\tau = \int_0^\tau C_{l_1}(\rho_t) dt \tag{2.86}$$

The thermodynamic cost of this dynamically generated coherence is appears in the lower bound on dissipated heat:

$$\beta Q \geq \Delta S + \frac{\bar{\gamma}_\tau^R C_\tau^2}{2\tau} \tag{2.87}$$

where $\bar{\gamma}_\tau^R$ is the time average characteristic relaxation rate written as $(\bar{\gamma}_\tau^R)^{-1} = \tau^{-1}\int_0^\tau (\Sigma_k \|L_k(t)\|_\infty^2)^{-1}$.

2.5 Quantum Confinement Effect

When a particle is trapped within a finite region comparable to its wavelength, the geometrical constraints restrict the allowed wavefunction, causing to the quantization of energy levels. This relation between wave characteristics of particles with the spatial domain geometry is called quantum confinement. The dynamics of such a quantum system are described by the time-dependent Schrödinger equation subjected to desired boundary condition:

$$i\hbar\frac{\partial}{\partial t}\psi(\mathbf{r},t) = -\frac{\hbar^2}{2m}\nabla^2\psi(\mathbf{r},t) + V(\mathbf{r},t)\,\psi(\mathbf{r},t) \tag{2.88}$$

where $\psi(\mathbf{r},t) = 0$ is the wavefunction of the particle that depends on position $\mathbf{r}$ and time t and h is Planck constant.

When the system size is comparable to the de Broglie wavelength, quantum confinement effects become more evident. The wave character of particles is quantified with their de Broglie wavelength $\lambda_{dB} = h/p$, where h is Plank constant and p is momentum. The de Broglie wavelength in three dimensions is (see (Pastor, 2019) for derivation).

$$\lambda_{th} = \frac{h}{\sqrt{2\pi m k_B T}} \tag{2.89}$$

where m, k_n, and T correspond to mass, Boltzmann constant, and temperature, respectively. This expression also includes the effect of thermalization in confined systems. At lower temperatures, the quantum effects become more pronounced. Due to limitations of the allowed quantum states and modification of the density of states, only a finite number of energy levels are populated at finite temperatures. These effects are not solely a consequence of the reduced system size but a fundamental

manifestation of how confinement geometry reshapes the energy spectrum and the resulting quantum behavior.

The following subsections begin with quantum boundary layer method, which is used to calculate the effective domain. Then quantum size and shape effect resulting from the change in effective domain is discussed.

2.5.1 Quantum Boundary Layers

The Schrödinger equation requires the implementation of boundary conditions when the particle is confined to a finite region. The Dirichlet boundary condition is where the wavefunction vanishes at the domain's boundary Ω. $\psi(\mathbf{r},t) = 0$ for $\mathbf{r} \in \Omega$. To satisfy the $\psi = 0$ condition, the wavefunction must decay rapidly near these boundaries over a short length, resulting in increased curvature ∇^2. Thus, the probability of the particle being localized in this small region is close to zero. Hence, the decay in probability density near the edges reduces the effective region accessible to the particle causing discrete energy levels and increasing energy.

The distribution of the particles is strongly affected by the decay of the wavefunction near the boundaries. When each wavefunction is weighted by its occupation probabilities, the combined effect of all wavefunctions in the boundary leads to a reduced particle density near those edges. This behavior reflects a fundamental quantum mechanical constraint on the system, with detailed calculations provided in (Sisman, Ozturk & Firat, 2007).

In equilibrium, the thermal density distribution is obtained from the ensemble average over quantum states. It is given by:

$$n(\mathbf{r}) = \sum_k f(E_k)|\psi_k(\mathbf{r})|^2, \tag{2.90}$$

where k is state index, E_k is energy value, $f(E_k)$ is distribution function (Boltzmann, Fermi-Dirac, or Bose-Einstein), $\psi_k(\mathbf{r})$ is eigenfunction. Thermal density distribution $n(\mathbf{r})$ appears approximately uniform in the interior of the domain but decays rapidly near the boundaries because wavefunction vanishes at the boundary. The sharp decay over a short distance defines the quantum boundary layer (QBL), within which the probability density becomes negligible.

To approximate this exclusion zone, QBL theory introduces an empty layer of thickness δ on each side of the confinement domain. (Aydin, 2020). Considering the ther-

mal density distribution and the decay at the boundaries, it has been showed that δ thickness is universal for the Maxwell-Boltzmann distribution (Firat & Sisman, 2009).

$$\delta = \frac{\lambda_{\text{th}}}{4} \tag{2.91}$$

This relation directly connects the boundary layer thickness to the quantum and thermal properties of the particles. Instead of solving the full Schrödinger equation, the QBL provides an approximation by adjusting the effective region of the confinement domain. In higher dimensions, this correction modifies the volume, area, and length as follows:

$$\begin{aligned} L_{\text{eff}} &= L - \delta N_V, \\ A_{\text{eff}} &= A - \delta P + \delta^2 N_V, \\ V_{\text{eff}} &= V - \delta A + \delta^2 P - \delta^3 N_V, \end{aligned} \tag{2.92}$$

where V, A, P, and N_V denote the volume, surface area, perimeter, and number of vertices of the domain, respectively. These corrections area obtained by considering, the exclusion on surface area (δA), overlap correction at edges ($\delta^2 P$), and the vertex contribution to excluded volume ($\delta^3 N_v$).

2.5.2 Quantum Size Effect

Quantum size effect is the term used for the changes that arise in the system due to changes in the size parameters of the system under quantum confinement conditions.

When the domain size is changed, all observables in the system are affected by this change. As the system size decreases, the energy levels become more discrete and the gaps between them start to increase. This situation can again be examined using the QBL approach. As the domain size decreases, the effect of the boundary layers increases relatively more compared to the total domain. This changes the statistical distribution of the particles and causes an increase in the ground state energy. This also takes into account the changes in the density of states and the variations in kinetic energy near the boundaries. As a result, the thermodynamic, optical, and transport properties of the system are influenced depending on its size.

For example, in the expression $V_{\text{eff}} = V - \delta A + \delta^2 P - \delta^3 N_V$, geometric volume V amplifies the impact of the subtraction terms involving δ. As a result, thermody-

namic observables calculated using V_{eff} exhibit significant deviations from classical counterpart V. Because, de Broglie wavelength has $\lambda_{th} \propto 1/\sqrt{T}$ relation with temperature, these deviations become especially prominent at low temperatures, where the boundary layer grow further inside the domain.

Quantum corrections become essential in nanoscale systems such as quantum dots, thin films, and nanowires, where confinement in one or more dimensions leads to size-dependent changes in energy levels and measurable quantum corrections to bulk behavior.

2.5.3 Quantum Shape Effect

The quantum shape effect refers to the influence of the domain's geometry, independent of its overall size, on the quantum and thermodynamic behavior of confined systems. Unlike the quantum size effect, which arises from changes in the geometric size parameters (V, A, L, P, N_V), the shape effect emerges due to size-invariant shape transformations (SIST).In order to understand the effect of shape-dependent behaviors, we must examine how modifications in confinement space affect the system's eigenspectrum (Aydin, 2023; Aydin & Sisman, 2023).

Time-dependent Schrödinger equation with Dirichlet Boundary condition Eq. 2.88 is mathematically equivalent to the Helmholtz equation $\nabla^2\psi + k^2\psi = 0$ where $k^2 = 2mE/\hbar^2$ represents the quantized momentum states. The solutions to this equation form a discrete spectrum of eigenvalues k_i that depends on the domain geometry Ω. When the Helmholtz equation is solved for domains with identical size but different shapes, their energy levels k_i will differ. This geometric coupling produces characteristic modifications in the system: non-uniform level scaling, ground state reduction, level splitting (Aydin, 2020).

Non-uniform level scaling, which creates uneven distribution due to shape change, occurs because different eigenfunctions respond differently to shape changes. The shape modifications affect the eigenfunction spectrum unevenly across the states. Higher energy states are more sensitive to this shape change. While total spectral density is preserved, energy level distribution changes, so the eigenvalues k_i do not scale uniformly (Aydin, 2023).

The ground state reduction occurs when the symmetry of the domain is broken due to shape transformations. As the domain's shape changes, certain regions have a larger effective domain and are less confined. The ground state is inclined to localize

in the larger regions because of its lower kinetic energy. Also, besides typical shape change, the overlapping quantum boundary layers near adjacent boundaries create an effective expansion for the ground state, making the particle behave as if in a larger domain (Aydin, 2023). The spectral modifications affect the operational behavior of thermodynamic properties. As the available volume changes, the partition function Z value is affected, and other thermodynamic properties are consequently affected. In the Fig. 2.1, a partition inside a rectangular domain is rotated quasistatically to observe the change in Z, F, U and S. Initially, when boundaries are far apart, the QBL of boundaries acts independently, making Z grow slowly. As boundaries approach and the boundary layers overlap, Z increases exponentially due to effective volume increase. Overlap boundary layers increase the effective region, which causes an increase in the partition function. Eventually, when boundaries get extremely close, the squeezed region becomes inaccessible. During the initial phase where boundary layers start to overlap, the effective volume grows, which leads to a sharp drop in free energy, entropy, and internal energy. This occurs because the ground state becomes increasingly dominant as it occupies the less confined regions, lowering the system's energy and disorder. When boundaries get extremely close, the squeezed region is excluded from the available domain. The entropy increases because the excluded region forces the states into a more disordered space.

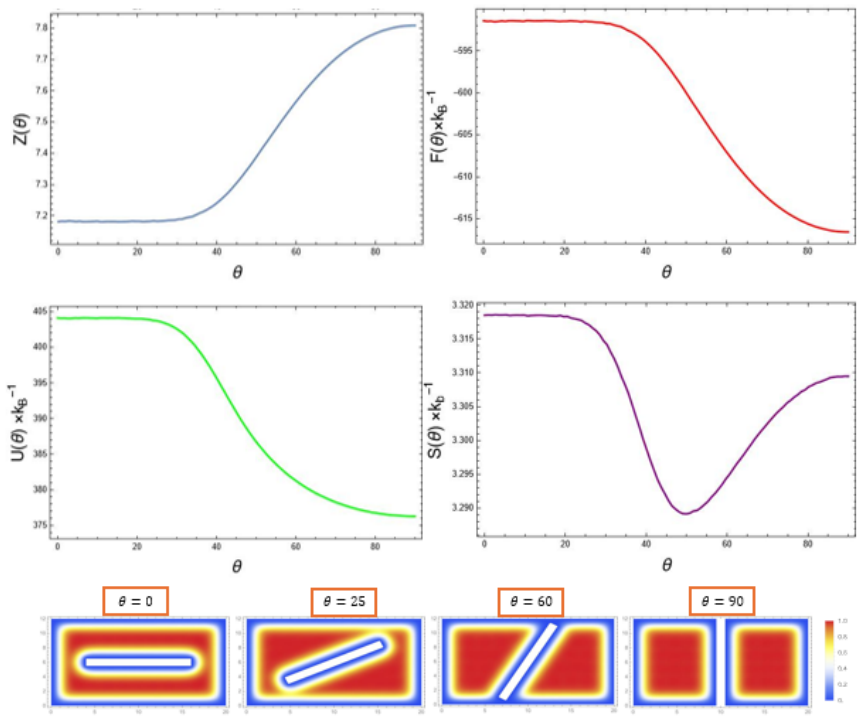

Figure 2.1 Partition function (Z), free energy (F), internal energy (U), entropy (S) during rotational SIST process. Below, the change in the thermal density distribution during rotation is shown. Between approximately 45–60 degrees, the effect of the change in effective volume within the system is reflected in the thermodynamic parameters.

the sudden decrease in the entropy is better understood when we check the energy levels Fig. 2.2. Avoided crossings in the energy levels begin to occur as the boundary layers approach each other. With the rotation of the partition, the eigenstates start to occupy larger areas where they can become more stable. This geometric reorganization leads to the formation of avoided crossings between the eigenstates (Aydin, 2023).

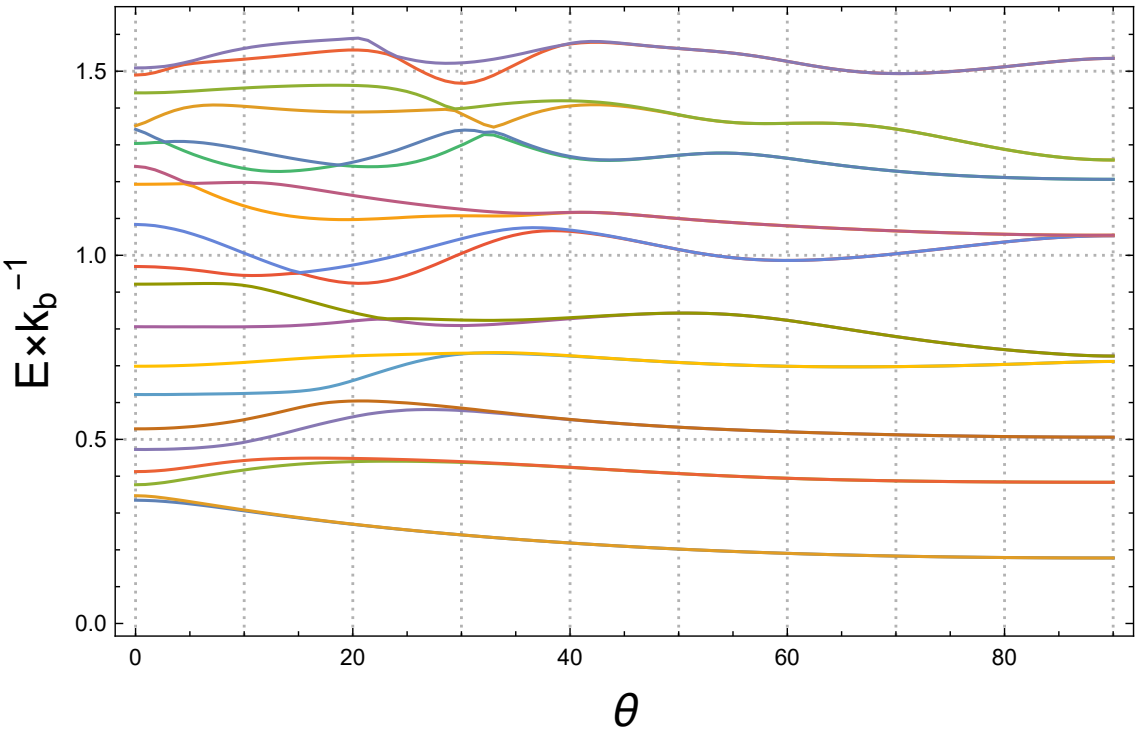

Figure 2.2 The state distribution, which starts in thermal equilibrium, leads to the formation of an avoided crossing during rotation (approximately in between 20-40 degrees) as the boundary layers begin to overlap.

3. QUANTUM SZILARD ENGINE

Measurement-based heat engines exploit the information while extracting work. The Szilard engine, which is a representation of Maxwell's demon thought experiment as discussed in Section 2.4.2, is a measurement-based heat engine that provides a profound example highlighting the connection between information extraction and thermodynamics (Szilard, 1929).

The classical Szilard engine consists of classical ideal single-particle gas in a box of volume V, a massless partition that can be inserted and removed, and an intelligent being like Maxwell's demon, which measures the particle's location. Initially, the partition is inserted into the box from the center, dividing it into two equal parts. The particle is trapped in either the left or right side of the box. Then, the demon performs a measurement to determine the particle's location. This 1-bit of information reduces the entropy by $\Delta S = k_B \ln 2$. Based on the measurement result, the demon attaches a weight to the partition. If the particle is on the left, the partition expands to the right due to pressure difference, and vice versa. As a result, work $W = k_B T \ln 2$ is extracted at the end of the expansion. Then, the partition is removed without any work, and the system returns to its initial state. According to Landauer's principle, erasing the information from the demon's memory increases the entropy by $\Delta S = k_B \ln 2$. Thus, the Szilard engine becomes an analogy to understanding the relation between information and measurement in thermodynamic processes.

Table 3.1 Thermodynamic changes during the classical Szilard engine cycle

Step	$\boldsymbol{\Delta F}$	$\boldsymbol{\Delta S}$	$\boldsymbol{W}$	$\boldsymbol{\Delta U}$
Insertion	0	0	0	0
Measurement	$-k_B T \ln 2$	$-k_B \ln 2$	0	0
Expansion	0	0	$+k_B T \ln 2$	0
Removal	$+k_B T \ln 2$	$+k_B \ln 2$	0	0
Full Cycle	0	0	$k_B T \ln 2$	0

While the classical formalism of information back-action establishes foundational principles, its extensions into the quantum domain offer a different perspective on the

underlying informational resources (Cai, Dong & Sun, 2012; Cuzminschi, Zubarev, Iordache & Isar, 2023; Elouard, Herrera-Martí, Huard & Auffeves, 2017; Peterson, Sarthour & Laflamme, 2020; Plenio & Vitelli, 2001; Sagawa, 2012b; Violaris & Marletto, 2022).

This chapter explores the thermodynamics of the quantum Szilard engine under quantum confinements effects. We introduce a finite-time formulation of the Szilard engine that designed to explore non-equilibrium dynamics of information-based engines.

3.1 Finite-Time Szilard Engine

The setup consists three elements, the system ($\mathcal{S}$), heat bath ($\mathcal{B}$) at constant temperature and the measuring device($\mathcal{M}$). The system is a one-dimensional particle in a box and a finite δ-potential barrier. The engine undergoes the four steps (Fig. 3.1):

- **Step I $\rightarrow$ II: (Insertion)** A finite δ-function potential barrier is inserted at the center of the box, partitioning the system into two compartments. The system remains coupled to the heat bath, and the barrier height increases from zero, driving the system out of equilibrium.
- **Step II $\rightarrow$ III (Measurement):** A strong or weak measurement is performed by $\mathcal{M}$. While the strong measurement localizes the particle to either the left (L) or right (R) compartment, the weak measurement partially localizes the particle. The measurement device is maintained at the same temperature as $\mathcal{B}$, but its thermal noise is neglected in the measurement. For strong projective measurements at the bath temperature this is fine, but for repeated weak measurements the pointer's back-action needs to be considered which we ignored here assuming it is weak.
- **Step III $\rightarrow$ IV Expansion:**
  - **Strong measurement regime:** After strong localization of the particle to one side, the barrier is shifted towards the outside of the box.
  - **Weak measurement regime:** The barrier undergoes incremental shifts, interrupted by repeated weak measurements. After each displace-

ment, the measurement outcome updates the localization probability and guides further expansion until the barrier reaches the wall.

- **Step IV → I:** The potential barrier is removed. The system returns to its initial configuration.

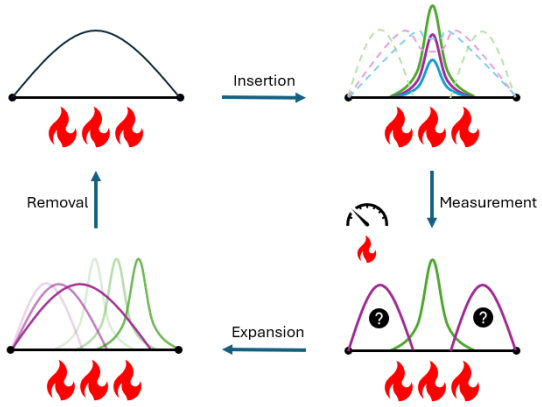

Figure 3.1 The schematic representation of the cycle. The ground state of the particle is illustrated as a representation.

We consider a particle of mass m confined to a one-dimensional box that extends from $x = 0$ to $x = L$, with a time-dependent potential barrier at the center, $x = L/2$. The system Hamiltonian is given by:

$$H(x,t) = -\frac{\hbar^2}{2m}\frac{\partial^2}{\partial x^2} + \alpha(t)\delta(x), \tag{3.1}$$

in which $\hbar$ is the reduced Planck constant and $\alpha(t)$ is time-dependent barrier strength.

The δ-potential barrier is investigated with rectangular function centered at $a = L/2$.

The rectangular barrier of height V_0 and width w is expressed using the Heaviside step function $H(x)$ as:

$$V_{\text{rect}}(x) = V_0\left[H\left(x - \left(\frac{L}{2} + dx - \frac{w}{2}\right)\right) - H\left(x - \left(\frac{L}{2} + dx + \frac{w}{2}\right)\right)\right], \tag{3.2}$$

where dx denotes a displacement of the barrier center from $L/2$.

The instantaneous eigenstates $|\psi_n(x,t)\rangle$ and corresponding eigenvalues $E_n(t)$ satisfies the time-dependent Schrödinger equation:

$$H(x,t)|\psi_n(x,t)\rangle = E_n(t)|\psi_n(x,t)\rangle, \tag{3.3}$$

with Dirichlet boundary conditions $\psi_n(0,t) = \psi_n(L,t) = 0$.

The system couples with the heat bath $\mathcal{B}$ at temperature $T = 1/k_B\beta$ at $t = 0$. After the coupling, the system's thermal equilibrium is disturbed by the heat bath and evolves according to LGKS master equation.

$$\dot{\rho}_s = -i[H_s, \rho_s] + \sum_k \gamma_k((N_k+1)(L_k\rho_s L_k^\dagger - \tfrac{1}{2}\{L_k^\dagger L_k, \rho_s\}) + N_k(L_k^\dagger \rho_s L_k - \tfrac{1}{2}\{L_k L_k^\dagger, \rho_s\})) \tag{3.4}$$

Here, $L_k = |\psi_{k-1}\rangle\langle\psi_k|$ are the jump operators that induce transitions between the adjacent energy levels of the system and the γ_k is the decay rate. $N(\omega_k) = \frac{1}{e^{\beta\hbar\Delta\omega_k - 1}}$ is the Bose-Einstein distribution function, where $\Delta\omega_k = (E_k - E_{k-1})/\hbar$ denotes the transition frequency corresponding the system energy spacing, as influenced by the interactions with the heat bath.

The Lindblad equation is designed for the Markovian evolution where the system interacts weakly with the heat bath with an Ohmic spectral density with decay rates $\gamma_k \propto \omega_k$.

During the insertion process (stage $1 \to 2$), the system evolves non-adiabatically under the combined influence of the time-dependent Hamiltonian (Eq. (3.1)) and the dissipative dynamics governed by the master equation (Eq. (3.4)). The driving parameter $\alpha(t)$ controls the insertion speed, with its specific functional form critically affecting the system's transition dynamics. Notably, rapid variations in $\alpha(t)$ lead to slower equilibration, as the system requires more time to adjust to sudden changes in the potential landscape.

Building on methods from (Das, Thomas & Jordan, 2023), where a finite-time Stirling engine is investigated, we simulate the insertion process via two different initial state; ground and thermal state.

Following the completion of the insertion process, we perform a projective measurement on the system. The left and right subspaces are defined by the projection operators:

$$P_{\mathrm{L}} = \sum_{n=0}^{N} |L_n\rangle\langle L_n| \quad P_{\mathrm{R}} = \sum_{n=0}^{N} |R_n\rangle\langle R_n| \tag{3.5}$$

where $\{|L_n\rangle\}$ and $\{|R_n\rangle\}$ span the left and right spatial regions, respectively (Davies et al., 2021).

We analyze two different measurement: strong and weak. These two measurement are encompassed within the general framework of POVMs, where a set of Kraus op-

erators M_k satisfies the completeness relation $\sum_k M_k^\dagger M_k = I$. The post-measurement state is given by (Erdman, Czupryniak, Bhandari, Jordan, Noé, Eisert & Guarnieri, 2025)

$$\rho(t+\Delta t) = \frac{M_k \rho(t) M_k^\dagger}{\mathrm{tr}[\rho(t) M_k^\dagger M_k]}. \tag{3.6}$$

For the n-level Szilard engine, we model the measurement process using a single Kraus operator of the form:

$$M_k = \sqrt{\kappa}\, P_{\mathrm{L}} + \sqrt{1-\kappa}\, P_{\mathrm{R}}, \tag{3.7}$$

where $\kappa \in [0,1]$ controls the measurement strength. As $\kappa = 1$, the measurement becomes strong, yielding maximal information about whether the particle is on the left. Conversely, when $\kappa = 0.5$ the measurement is uninformative, corresponding to a minimal disturbance of the system. Intermediate values of κ enable tunable weak measurements, allowing partial information gain while decreasing state disturbance.

This formulation captures the fundamental trade-off between information gain and measurement disturbance that is crucial for the Szilard engine operation. The measurement strength κ can be experimentally controlled through parameters like interaction time or coupling intensity in realistic implementations.

Following the measurement phase, the system undergoes expansion, which proceeds differently depending on the measurement regime. In the case of the strong measurement, the potential barrier is continuously shifted toward the outer wall. Under a weak measurement regime, the expansion is performed sequentially: after each small displacement of the barrier, the measurement strength κ is updated. And another weak measurement is applied with the updated measurement strength. This measurement-feedback process is repeated iteratively, guiding the gradual expansion until the barrier reaches the edge of the box.

Through out the entire operations we monitor thermodynamic evolution of the particle. The changing energy landscape and quantum state dynamics are captured through several key quantities.

The internal energy U of the system:

$$U(t) = \mathrm{tr}[H(t)\rho(t)] = \sum_n \underbrace{E_n(t)}_{\substack{\text{Shifting} \\ \text{energy levels}}} \underbrace{p_n(t)}_{\substack{\text{Changing} \\ \text{populations}}} \tag{3.8}$$

reflecting both the shifting energy spectrum and state probability adaptation. Here, $p_n(t)$ are the occupation probability.

The entropy S quantifies information loss and irreversibility during the non-adiabatic process due to population adaptation of energy levels. It is given as:

$$S(t) = -k_B \operatorname{tr}[\rho(t) \ln \rho(t)] = -k_B \sum_n \underbrace{p_n(t) \ln p_n(t)}_{\substack{\text{population change} \\ \text{disorder}}} \tag{3.9}$$

Entropy production caused by both population change $p_n(t)$ and quantum coherence of $\rho(t)$.

From the definitions of internal energy and entropy, the free energy F in non-equilibrium is:

$$F(t) = U(t) - TS(t). \tag{3.10}$$

The relation between F and work is $W_{irr} \leq -\Delta F$ determines the bounds the extractable work. For reversible process the equality holds.

The incremental work during expansion is results from changes in Hamiltonian $H(t)$ and the system's state remains unchanged instantaneously. Applying forward difference method to Eq. 2.56 gives the incremental work ΔW in Δt time step:

$$\Delta W = \operatorname{tr}\left(\frac{dH}{dt}\rho(t)\right) = \operatorname{tr}\left[\Delta H(t)\, \rho(t)\right] \tag{3.11}$$

The incremental heat reflects energy change due to changes in the system's state $\rho(t)$ at fixed Hamiltonian:

$$\Delta Q = \operatorname{tr}\left[H(t)\, \Delta\rho(t)\right] \tag{3.12}$$

These definitions satisfy the first law of thermodynamics $\Delta Q = \Delta U - \Delta W$.

The second law constrains heat dissipation in terms of entropy production:

$$\delta Q \geq T\, dS, \tag{3.13}$$

with equality for reversible processes. Landauer bound follows this principle when we applied it to the erasure of information. For non-equilibrium systems, the entropy production $\Sigma_\tau = -\Delta S + \beta Q \geq 0$ (where $\beta = 1/(k_B T)$) reveals irreversibility from both population relaxation and quantum coherence decay and generalize the second law to finite-time operations. The excess entropy produced by irreversible operations $\Sigma_\tau > 0$ reflects their deviation from equilibrium. For quantum information erasure, the minimum heat dissipation is given by Eq. 2.82.

The complete thermodynamic cycle reveals how quantum coherence, embedded in the off-diagonal elements of $\rho(t)$, modifies work extraction and efficiency compared to classical expectations. These effects become particularly significant when analyzing the full engine operation across all phases.

In addition, to characterize quantum coherence throughout the thermodynamic cycle, we employ three complementary approaches. The standard relative entropy and ℓ_1-norm coherence measures are defined respectively as:

$$C_{\text{rel}}(\rho) = S(\rho_{\text{diag}}) - S(\rho), \quad C_{\ell_1}(\rho) = \sum_{i \neq j} |\rho_{ij}|, \tag{3.14}$$

where ρ_{diag} represents the state with all off-diagonal elements set to zero. These measures satisfy all axiomatic requirements for proper coherence quantifiers.

To characterize quantum coherence in our system, we analyze the thermally weighted coherence:

$$C_w = \sum_{i,j} \rho_{i=j} |\rho_{i \neq j}|, \tag{3.15}$$

which we specifically designed to track the contribution of initial state coherence throughout the evolution and to give emphasis on the quantum coherence accumulated in states with high thermal occupation. While this measure may not satisfy all general requirements for coherence quantification mentioned in (Baumgratz et al., 2014), it serves our particular purpose of monitoring how initial quantum coherence propagate and influence the thermodynamic process. The measure compares the weighted magnitude of off-diagonal elements against population terms, providing insight into how initial superposition of most relevant states affect the system dynamics. This proves particularly useful for understanding the role of initial coherence in work extraction and other thermodynamic quantities.

Finally, we evaluate the non-adiabatic work contribution by comparing the work performed during the quasistatic process (W_{qs}) with that of the finite-time process (W_{ft}).

$$\Delta W_{\text{non-adiabatic}} = W_{\text{ft}} - W_{\text{qs}} \tag{3.16}$$

In the following sections, we analyze the Szilard engine with two different initial conditions; thermal and ground state. For each case, we determine the optimal parameters to maximize efficiency and examine the trade-offs between temperature, dissipation rate, insertion speed,acceleration, partition width, and efficiency.

The system is modeled using dimensionless parameters to simplify numerical calculations while preserving physical interpretation. The physical constants are scaled

such that $\hbar = 1$, Boltzmann constant $k_B = 1$ and the electron mass $m = 1$. The position space is discretized into $n = 30$ grid points over the length $L = L_{\mathrm{SI}}/L_0$ where $L_{\mathrm{SI}} = 10\mathrm{nm}$ is the length of the box in SI units and L_0 is reference length that is obtained from the characteristic energy scale $E_0^{\mathrm{SI}} = {\hbar_{\mathrm{SI}}}^2 / 2 m_{\mathrm{SI}} L_0^2$.

The relation between natural units and SI units of temperature is $T_{\mathrm{SI}} = T \times E_0^{\mathrm{SI}}/k_B^{\mathrm{SI}}$.

The Markovianity conditions are naturally satisfied in this framework through the following physical constraints: the dissipation rate in SI units $\gamma_0^{\mathrm{SI}} = \gamma_0/t_0$ is chosen to be much smaller than the system's characteristic energy gap $\Delta E/\hbar$, ensuring weak coupling between the system and bath. Here, ΔE represents the smallest energy difference between quantum states, which for this system scales as $\Delta E \sim E_0$. Additionally, the bath's cutoff frequency ω_c inherently exceeds γ_0^{SI} due to the Lindblad formalism's assumption of a memoryless environment, where the bath correlation time $\tau_B \sim 1/\omega_c$ is negligible compared to the system's dynamical timescales. The Born approximation further holds since $\gamma_0^{\mathrm{SI}} \ll k_B T/\hbar$, guaranteeing that the bath remains unperturbed by the system. These conditions collectively enforce Markovian dynamics, validating the use of the LGKS master equation(Eq. 3.4) for this setup.

3.1.1 Initial Thermal State

The system initially is in Gibbs's state, the initial state of the system is:

$$\rho(0) = \frac{e^{-\beta H(0)}}{Z}, \tag{3.17}$$

where $Z = \mathrm{tr}(e^{-\beta H(0)})$ is partition function and $\beta = 1/k_B T$ is inverse temperature. At $t = 0$, the system is coupled to the heat bath.

As the barrier strength $\alpha(t)$ changes rapidly the finite-time modification of the potential leads to different degrees of departures from equilibrium thermodynamics. The distinct non-adiabatic dynamical signatures produced by $\alpha(t)$ is followed with fidelity. The fidelity measures the similarity between the system's actual state and the thermal state corresponding to the instantaneous Hamiltonian, thus serving as an indicator of how far the system is from equilibrium.

$$F(\rho(t), \rho_{th}(t)) = \mathrm{tr}\left[\sqrt{\sqrt{\rho_{\mathrm{th}}(t)}\,\rho(t)\,\sqrt{\rho_{\mathrm{th}}(t)}}\right]. \tag{3.18}$$

The populations are calculated in energy basis ρ_e:

$$p_n(t) = \langle \psi_n(t) | \rho_e(t) | \psi_n(t) \rangle \tag{3.19}$$

The insertion strength is chosen as $\alpha(t) = ct$, where c corresponds to insertion acceleration.

To identify the maximum achievable efficiency of the quantum Szilard engine, we conducted a systematic parameter scan over temperature T, dissipation rate γ_0, and insertion acceleration c. The ranges of these parameters were chosen to encompass the physically relevant, efficient operating regimes of the engine. In (Fig. 3.2), the three plots illustrate how efficiency changes with each control variable during this optimization process. The approach involves varying one parameter at a time while keeping the others constant, allowing the influence of each parameter on efficiency to be isolated and the optimal value to be identified. First, the insertion speed c is varied while keeping T and γ_0 fixed. This gives the value of c that maximizes efficiency for the chosen operating conditions. Next, c is fixed at this optimal value, and the hot bath temperature T is varied to find the temperature that yields the highest efficiency under the updated settings. Finally, with both c and T fixed at their respective optimal values, the dissipation rate γ_0 is varied to determine its optimal point. This procedure is applied because testing all the parameters together is not computationally feasible.

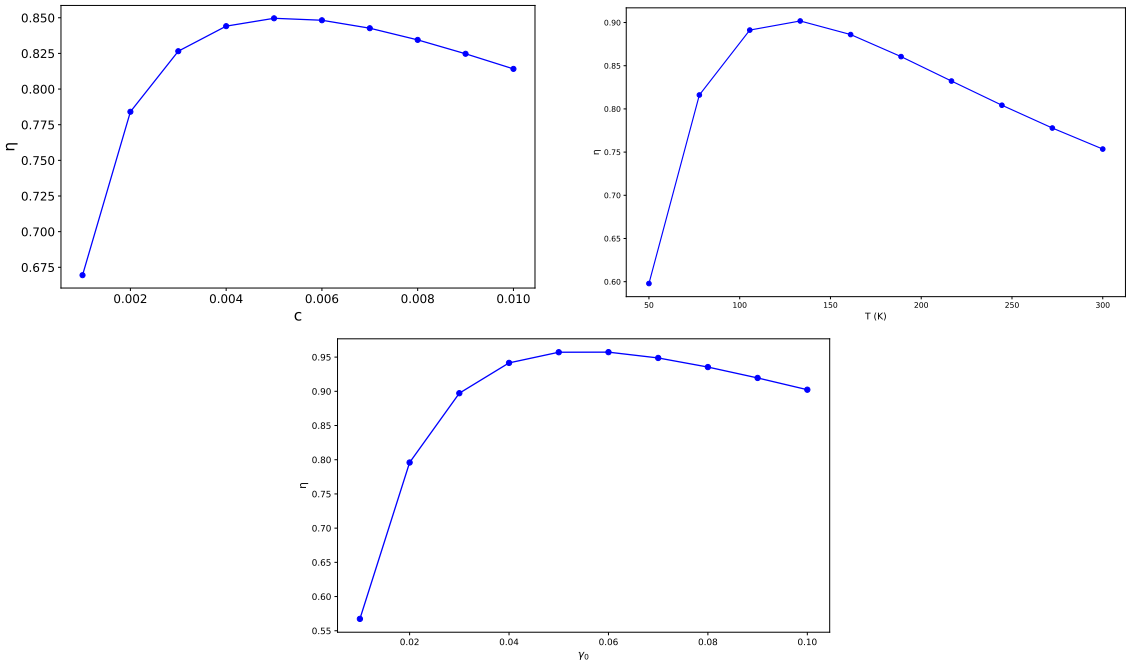

Figure 3.2 The parameters with respect to efficiency η in order of: (a) c vs η, (b) T vs η, (c) gamma vs η

From this procedure, the parameters are chosen to be $c = 0.05$, $T = 133$K, and $\gamma_0 = 0.06$ for $n = 18$ energy levels. Using these parameters, I then observe the thermodynamic changes in the system, starting from fidelity (Fig. 3.3).

During insertion, since the dissipation rate γ_0 and c are small in the finite-time regime, the equilibrium state is preserved. However, fluctuations caused by measurement disturb the equilibrium. During expansion, the system approaches equilibrium again.

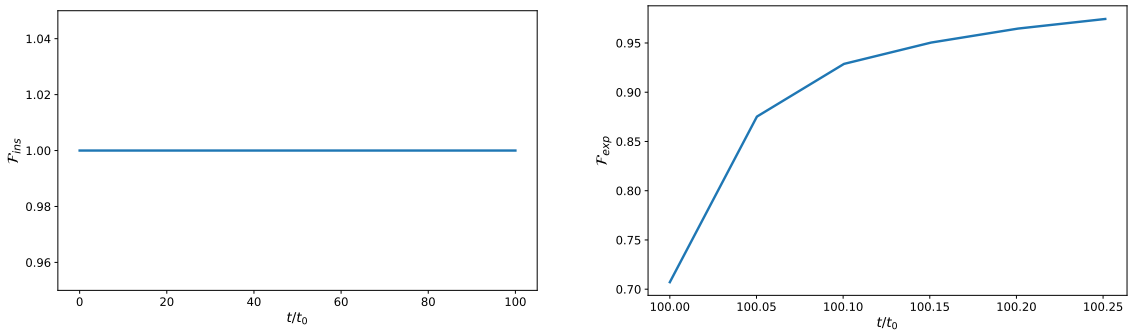

Figure 3.3 The fidelity when the initial state is chosen as thermal: (a) insertion (b) expansion

Under ideal quasistatic conditions, the populations track the equilibrium Gibbs distribution $p_n(t) = \frac{e^{-\beta H(t)}}{Z(t)}$. Since the equilibrium is not disturbed during insertion, the population graph gives the same results for both the quasistatic (dashed lines) and finite-time (solid lines) cases. (Fig. 3.4-a).The energy level diagram at the end of the insertion shows that the system is in a degenerate state.(Fig. 3.5-a). The avoided crossings in the spectra of the expansion process, as seen in Fig. 3.4-b, are a hallmark of the quantum shape effect (Aydin, 2023).

During expansion, we focus only on the finite-time regime. Because, after the measurement, the use of the Gaussian approximation to the Dirac delta potential causes a discontinuous separation of the box, which causes a significant error in the quasistatic regime.

In the finite-time expansion, non-adiabatic transitions occur due to rapid barrier insertions. Fidelity indicates the deviations from equilibrium.

The non-adiabatic effects manifest through two distinct mechanisms. First, the coherent dynamics generates off-diagonal elements in the energy eigenbasis through the unitary term $-i[H(t), \rho(t)]$, due to non-commuting terms of the $H(t)$. Second, the dissipator attempts to restore the system towards equilibrium by suppressing these coherence at a rate determined by the γ_k coefficients. The competition be-

tween these processes leads to the finite-time population dynamics observed in the simulation.

Throughout expansion energy levels exhibit avoidant crossing, unlike the insertion case. This behavior arises from the SIST in the system. As the partition moves, the boundary layer of the partition and the outside wall get closer, which decreases the effective length of the box. This shape transformation leads to ground state reduction; as a result, the ground state becomes energetically more favorable, and the population increases. This redistribution of state due to ground state reduction is driven by the SIST.

The observed population dynamics and energy level shifts are influenced not only by the insertion speed and non-adiabatic transitions but also by this modification of the effective confinement length and the shape due to the barrier's finite size (Fig. 3.5)

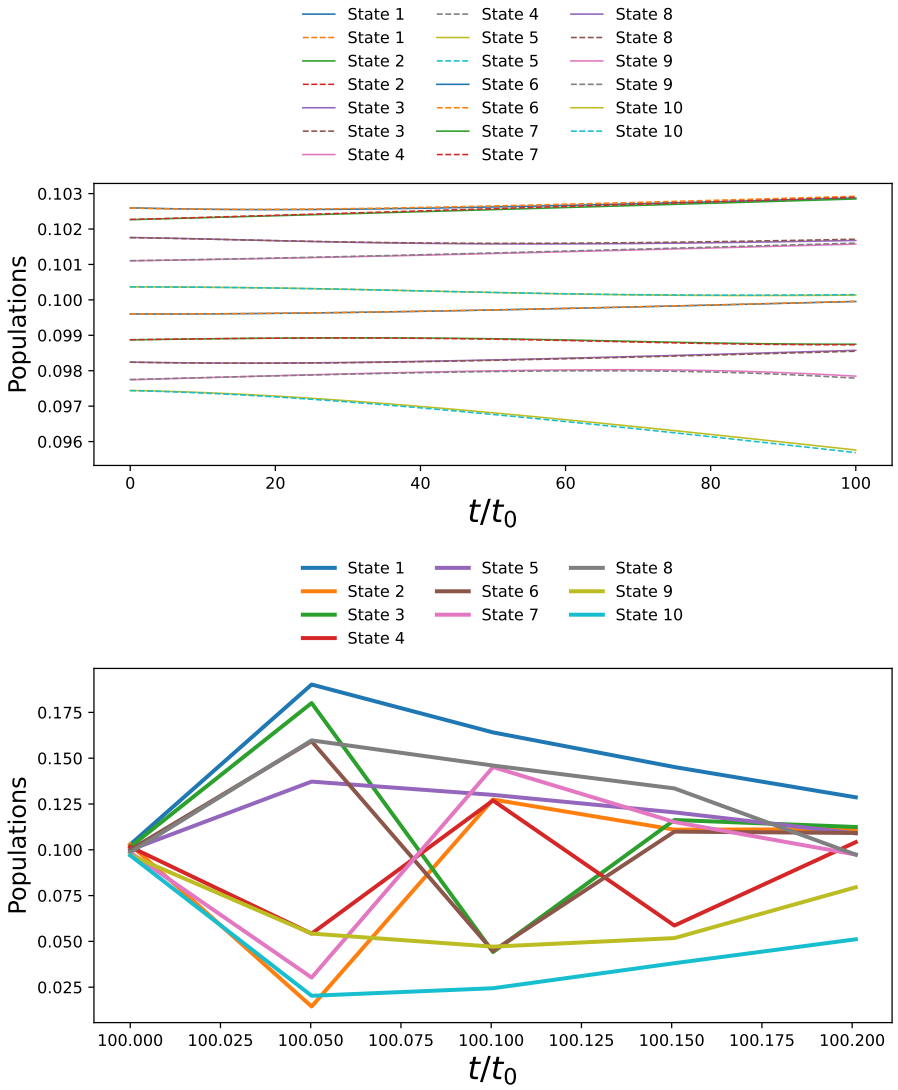

Figure 3.4 Population: (a) insertion (b) expansion

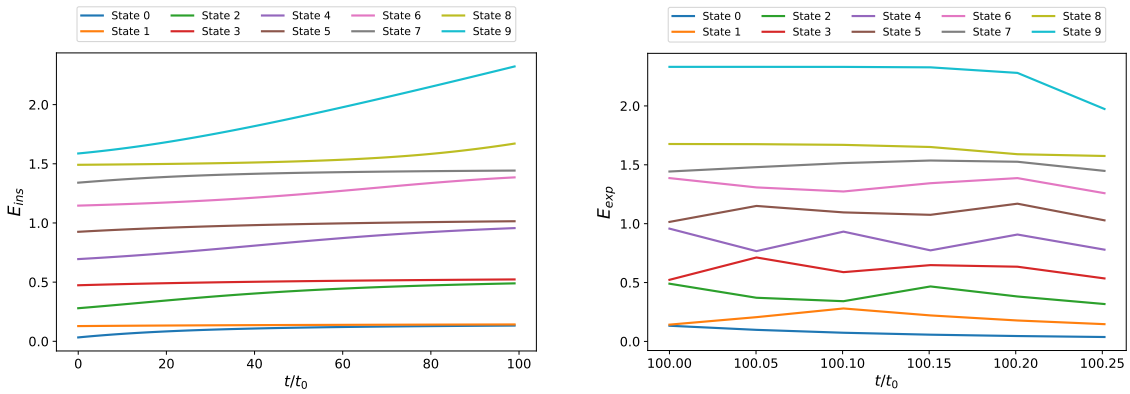

Figure 3.5 Energy levels: (a) insertion (b) expansion

An important consideration in this context is the size effect resulting from barrier insertion. The insertion effectively divides the original box into two smaller compartments. Moreover, the finite width and height of the potential barrier reduce the available effective volume for the particle. This leads to a decrease in the effective length of each compartment, which alters the energy spectrum beyond just splitting the domain. The reduction of the effective length increases the energy eigenvalues because the particle is more tightly confined.

The Fig. 3.13 shows the effect of finite-time behavior on internal energy U, free energy F, and entropy S. We compare the quasistatic insertion process with the finite-time insertion.

In finite-time insertion, U, F and S shows the same behavior as quasistatic cases due to preservation of equilibrium.

The internal energy U, which changes proportionally with the population and the shifting energy levels, increases due to the small changes occurring in these values. Similarly, we observe that the entropy, which varies inversely with the population, decreases. However, the change in internal energy dominates over the change in free energy, causing the free energy to increase.

In the finite-time regime, the slight difference on the entropy is result of decoherence generated by the heat bath. The effect of coherent terms is better understood when we check the relative entropy of coherence and the relative work of coherence (Fig. 3.15).

In the expansion process, the ground state energy population increases, which causes a decrease in the internal energy. The increase in internal energy is compensated by a corresponding increase in entropy, resulting in no substantial reduction in free energy.

At the end of the expansion, the ground state population of the system increases. This is due to the decrease in the ground state energy level. However, as the overlap areas of the boundary layers decrease again, the ground state population increases once more. This behavior is clearly reflected in the change of internal energy.

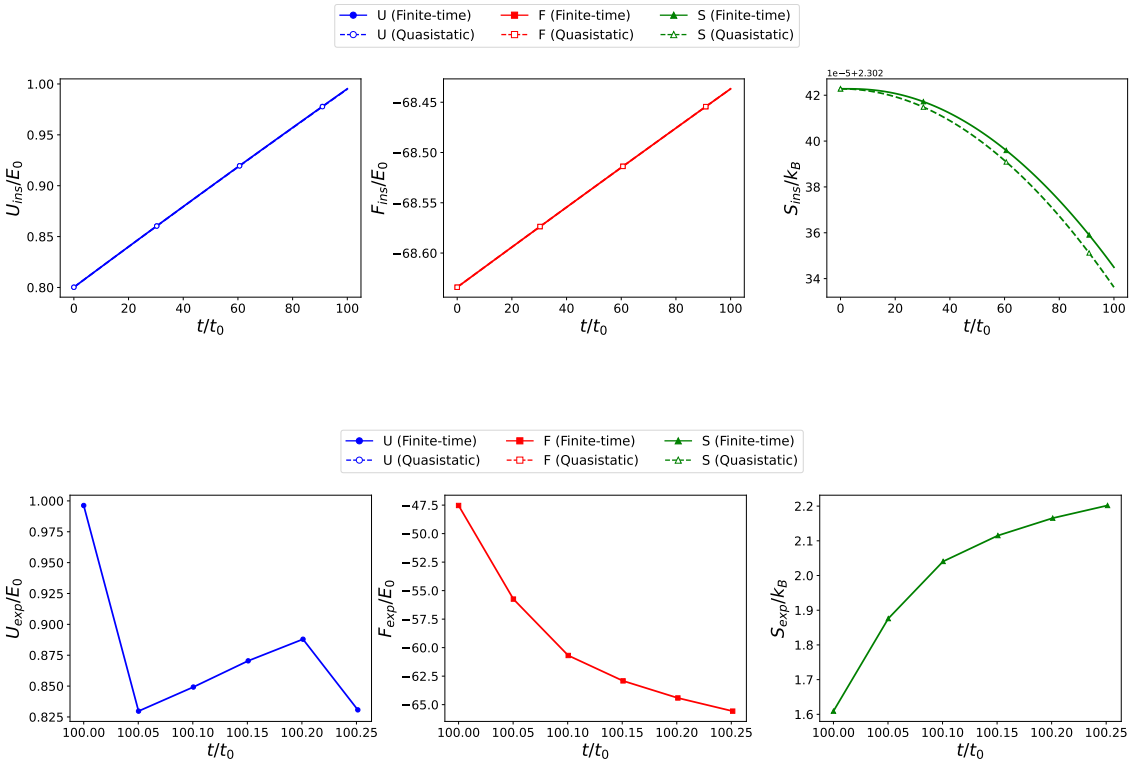

Figure 3.6 Comparison of internal energy U, free energy F and the entropy S: (a) insertion (quasistatic and finite-time). (b) expansion (finite-time).

During insertion process system does work due to changing potential term in Hamiltonian, also the heat is applied due to change in population to adapt the new Hamiltonian (Fig. 3.14). When we check the work contribution of the coherent terms $W_{coh} = \mathrm{tr}(\Delta H \rho) - \mathrm{tr}(\Delta H \rho_{diag}) = 0$ show that the work contribution is not due to extra coherence generation, but because of the extra finite-time non-adiabatic transition.

During the expansion, the system performs work on the surroundings, and the amount of this work varies over time. The same can be said for the dissipated heat.

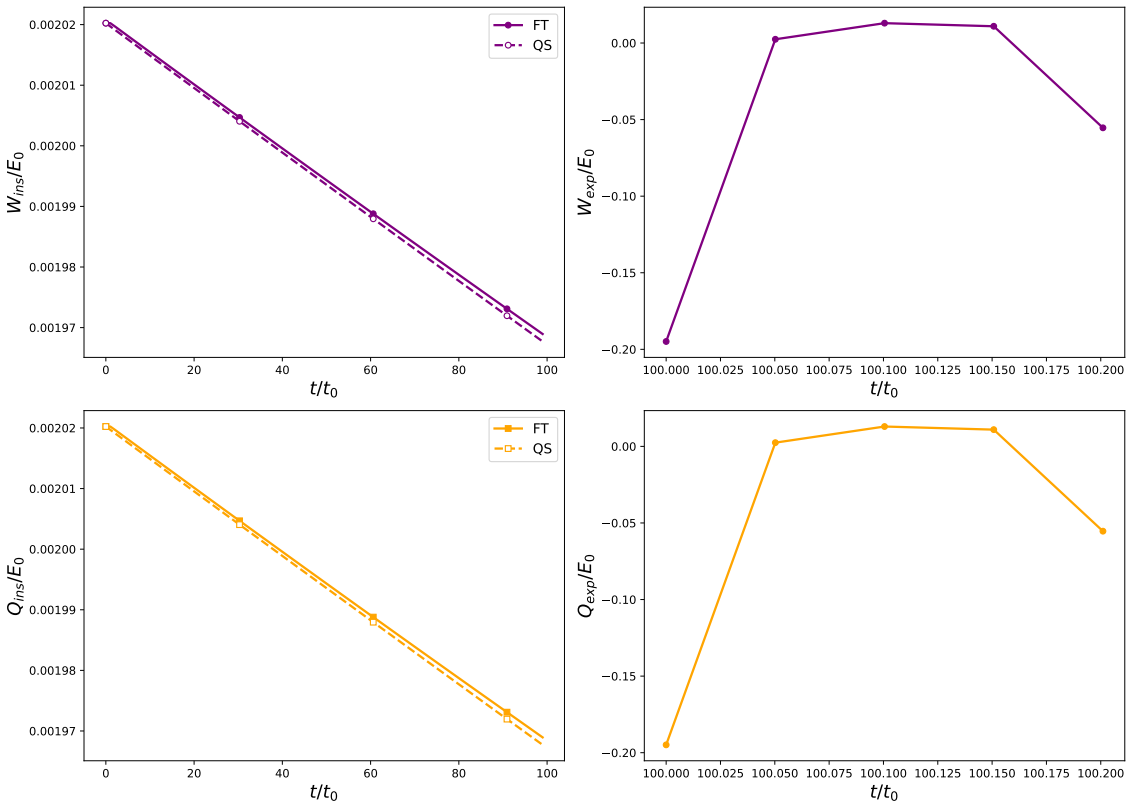

Figure 3.7 Work and heat change in each step. (first column) insertion, (second column) expansion

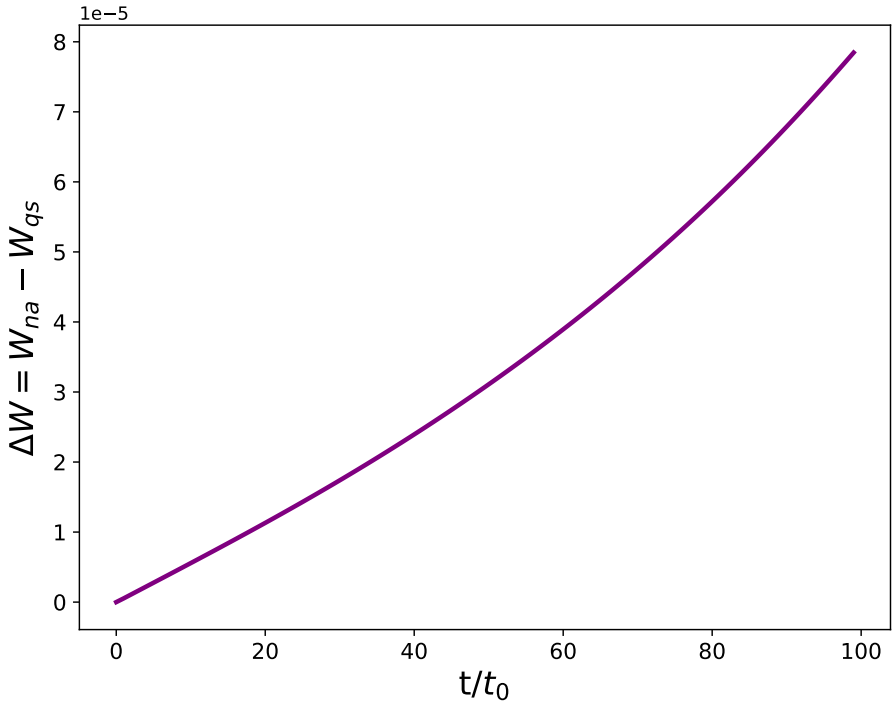

Figure 3.8 The difference in work changes between the nonadiabatic and quasistatic cases

Fig. 3.9 shows different type of the coherence measure in the system. l_1 coherence measure shows the weight of the off diagonal terms in the energy basis. It is a direct count of the coherence in the system. On the relative entropy we can see the entropy contribution of the coherent terms in the system. C_w measure indicates the coherence contribution of lower states population.

Entropy production can be decomposed into classical and quantum cost as in Eq. 2.85. Using the dephasing map classical entropy change $\Delta S = S_{cl} + S(\rho||\rho_{diag})$ from population redistribution can be obtained as:

$$\Delta S_{cl} = S(\Pi(\rho(t_0))) - S(\Pi(\rho(t))) \tag{3.20}$$

and the relative entropy of coherence lost to the environment:

$$S(\rho||\rho_{diag}) = S(\rho) - S(\rho_{diag}) \tag{3.21}$$

At the end of the expansion, the remaining coherence in the system can be used to extract work Eq. 2.79. This work can then be utilized during the partition insertion step in the next cycle. However, during the removal process, as the system tries to return to its initial thermal equilibrium state, these coherences are lost. Therefore, there are currently two possible ways to extract work from coherence: either by employing an alternative mechanism during removal to extract work from the remaining coherence, or by better defining the system's initial and final states. For this reason, the removal process is not included in this thesis.

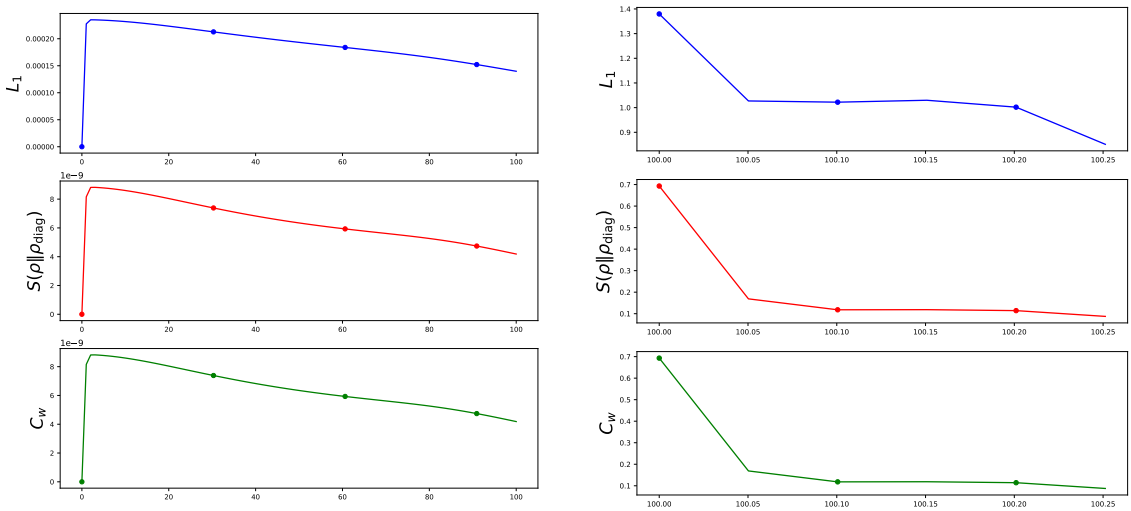

Figure 3.9 Comparison of coherence measures: (first column) insertion (quasistatic + finite-time), (second column) expansion (after measurement)

After the partition is removed from the system, the changes required for the system to return to its initial state (erasure) are determined. The change in internal energy can be found using the difference between the system's initial and final states, $U_{\text{eras}} = U(t_{\text{final}}) - U(0)$. Since the system Hamiltonian remains constant after the partition is removed from the box, the system neither performs work nor receives work during erasure. According to the first law, the change in internal energy equals the heat change $U_{\text{eras}} = Q_{\text{eras}}$.

The efficiency is defined as:

$$\eta = \frac{W_{\text{total}}}{Q_{\text{ins}}}. \tag{3.22}$$

The final results of the changes in thermal quantities, obtained using Table 3.3, are given in Table 3.2.

Table 3.2 Thermodynamic quantities for each stage of the cycle

Quantity	**Insertion**	**Measurement**	**Expansion**	**Erasure**	**Total**
ΔU	0.1950	0.0011	-0.1655	-0.0305	0.0000
ΔF	0.1974	20.9038	-18.0364	-3.0647	0.0000
ΔS	-0.0001	-0.6931	0.5926	0.1006	0.0000
Total Work	0.1975	0.0000	-0.2239	0.0000	-0.0264
Total Heat	-0.0024	0.0011	0.0584	-0.0305	0.0264

Table 3.3 Parameters for initial thermal state scenario

n	**c**	γ_0	**T (K)**	η
10	0.05	0.06	133	0.44

3.1.2 Initial Ground State

To minimize scattering and tunneling effects originating from higher energy levels, the system was initialized in the ground state, and the insertion, measurement, and expansion procedures were applied in the same manner.

$$\rho(0) = |\psi_0(0)\rangle\langle\psi_0(0)| \tag{3.23}$$

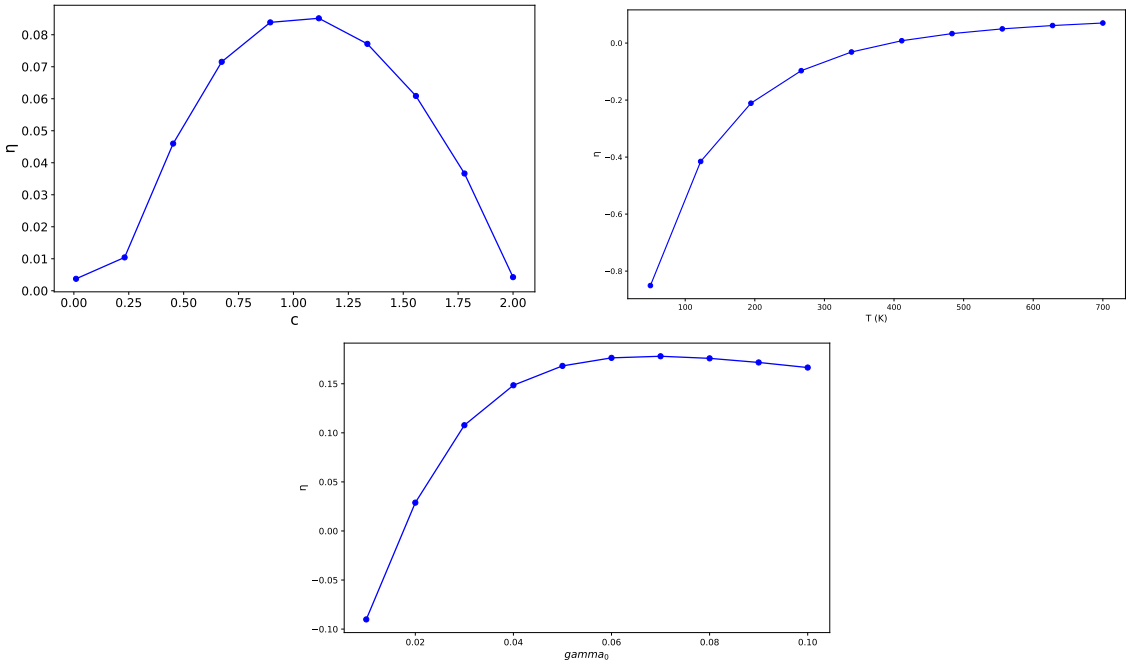

Figure 3.10 The parameters with respect to efficiency η in order of: (a) c vs η, (b) T vs η, (c) gamma vs η

In this procedure, the parameters are set to $c = 1.15$, $T = 300\,\mathrm{K}$, and $\gamma_0 = 0.07$ for $n = 18$ energy levels. These parameters do not yield the maximum efficiency, as testing all parameter combinations is computationally infeasible.

Using these parameters, the thermodynamic changes in the system are examined, beginning with fidelity. Since the system starts from the ground state, it is not in thermal equilibrium during insertion. Towards the end of the insertion, it reaches thermal equilibrium.

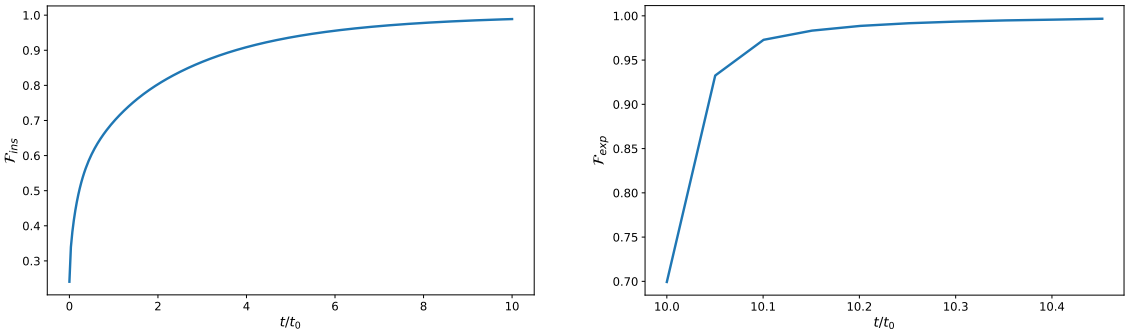

Figure 3.11 Fidelity: (a) insertion (b) expansion

The system, initially in the ground state, is connected to the heat bath, leading to an increase in the populations of the higher energy levels during the insertion stage until a thermal distribution is reached. During the expansion, the populations of

the lower energy states initially increase due to the reduction of the ground state energy caused by SIST. Subsequently, the system returns to a thermal distribution.

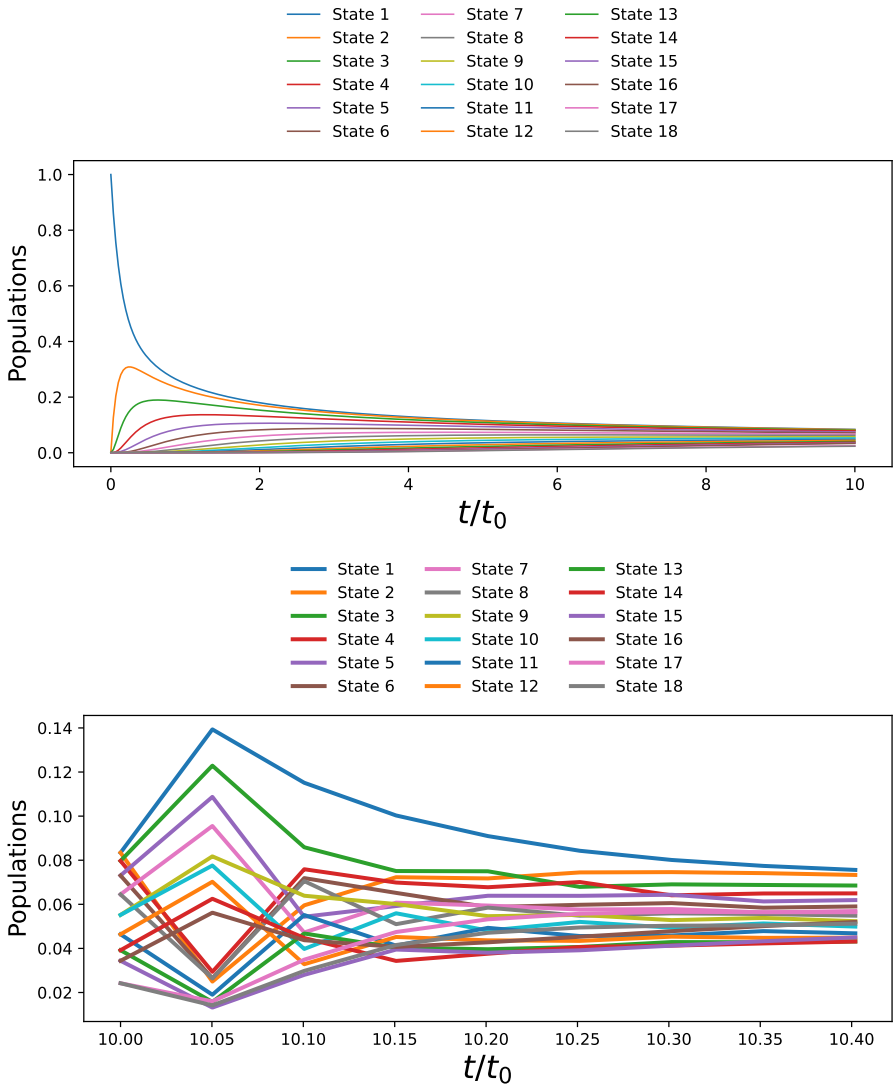

Figure 3.12 Population: (a) insertion (b) expansion

The deviation of the system from equilibrium during insertion leads to differences between the quasistatic and finite-time cases. The main source of this difference is that, in the quasistatic case, the system is in thermal equilibrium, resulting in a different population distribution.

The internal energy, U, exhibits a characteristic dip during the expansion phase. This transient decrease is attributed to the rate of work extraction momentarily exceeding the rate of heat absorption from the reservoir. The subsequent relaxation of U back to its initial thermal equilibrium value upon completion of the expansion signifies a final re-thermalization process.

As predicted by the second law, the free energy, F, decreases monotonically throughout the expansion. The initial steep decline corresponds to a period of rapid relaxation when the system is furthest from its final equilibrium. As the system approaches the new equilibrium state in the expanded volume, the rate of change of F diminishes, eventually plateauing as the potential for further work extraction is exhausted.

The system's entropy, S, increases and stabilizes at a new, higher value. This increase is composed of two contributions: the change in configurational entropy due to the expanded volume, and, crucially, the entropy produced internally due to the irreversibility of the finite-time process.

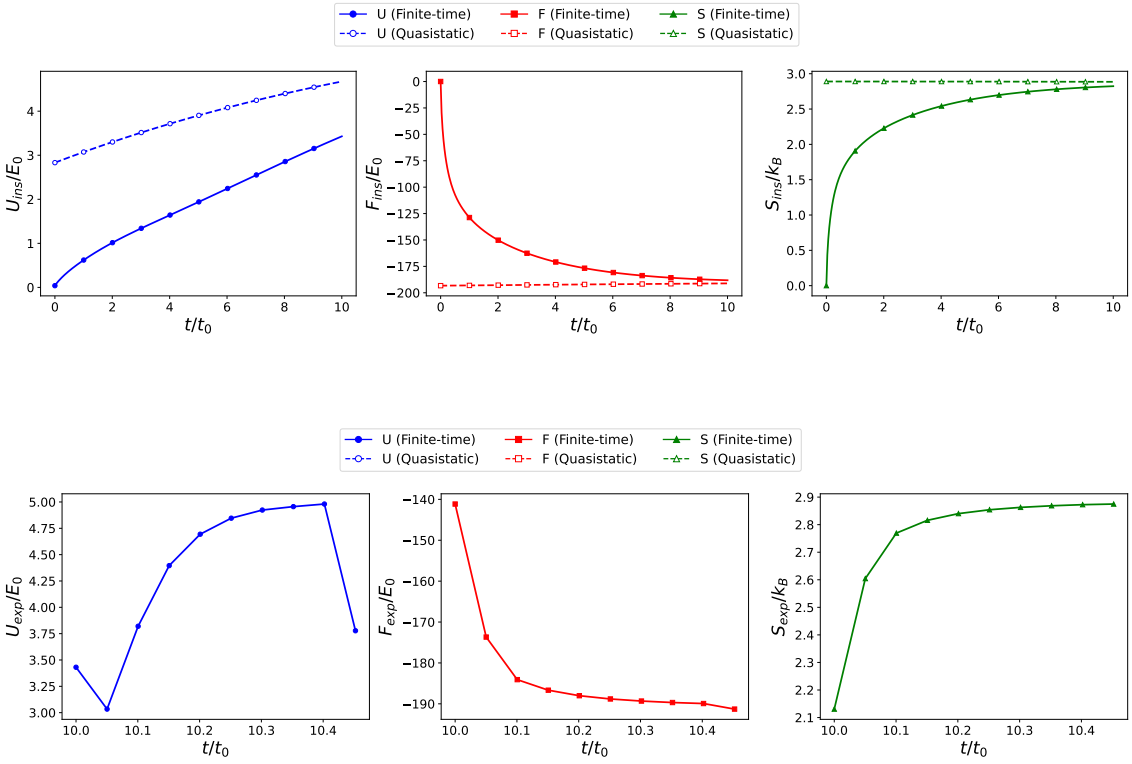

Figure 3.13 Comparison of internal energy U, free energy F, and entropy S: (a) insertion (quasistatic and finite-time), (b) expansion (finite-time)

During the finite-time insertion, the work cost per increment behaves non-monotonically, in stark contrast to the smooth profile of the quasi-static benchmark. This behavior is a direct consequence of non-adiabatic dynamics. The final increase in work cost before the insertion completes can be interpreted as a dynamic rebound effect, where an out-of-equilibrium quantum state exerts transient pressure on the barrier as it comes to rest. The total work cost is greater than the reversible limit ($k_B T \ln 2$), with the excess work being dissipated as heat due to quantum friction.

"The profile of the extracted work per increment during the finite-time expansion is highly non-uniform. The initial peak corresponds to the maximum pressure exerted by the particle at the start of the expansion. We observe a subsequent dip in the work rate, which we attribute to transient, non-equilibrium effects; the particle's quantum state lags behind the rapidly retreating partition, temporarily reducing the force exerted and the power output. The process concludes with a sharp drop in work extraction as the partition's velocity and the particle's pressure both approach zero.

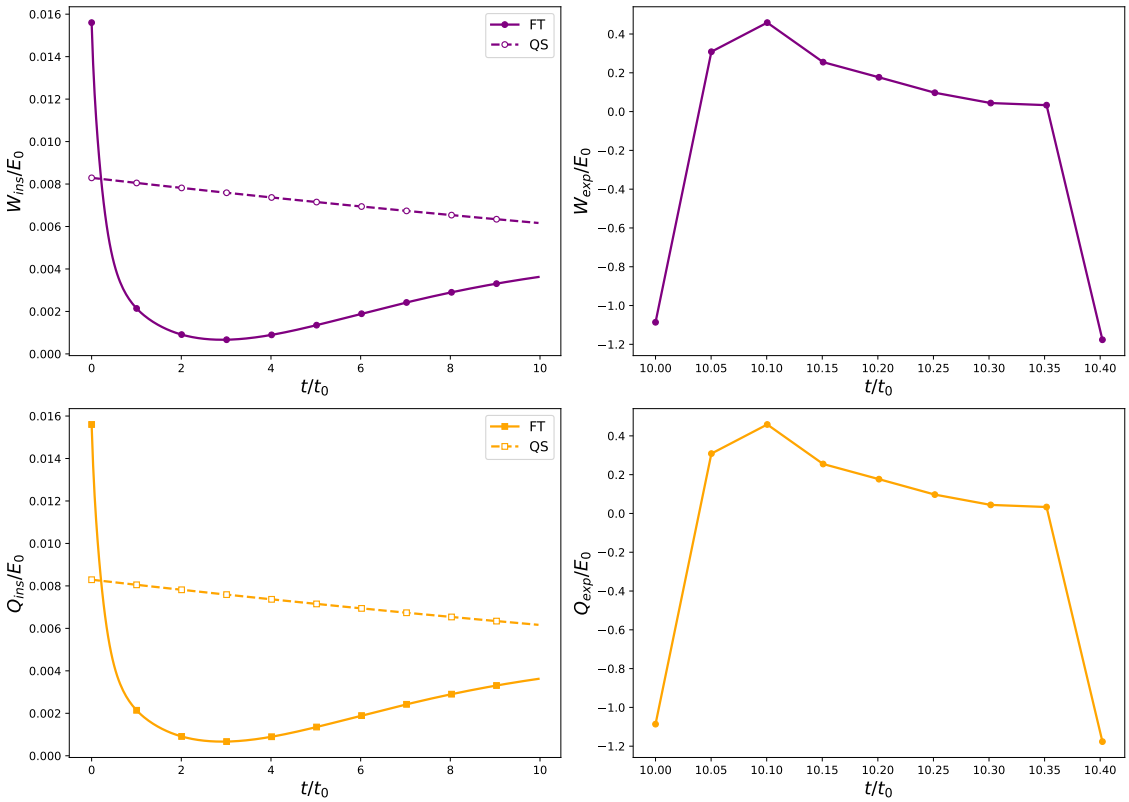

Figure 3.14 Work and heat change in each step: (first column) insertion, (second column) expansion

To quantify the thermodynamic cost of finite-time operation, the difference between the work extracted in the non-adiabatic and quasi-static protocols, $\Delta W = W_{\mathrm{na}} - W_{\mathrm{qs}}$, was analyzed. This quantity, representing the work lost to dissipation, is observed to decrease nearly linearly as the expansion progresses. This linear trend suggests that the rate of entropy production due to quantum friction is approximately constant for the given expansion protocol. The final negative value of this difference at the end of the process quantifies the total energy that was irreversibly dissipated as heat instead of being converted into useful work, highlighting the energetic cost required to achieve non-zero power.

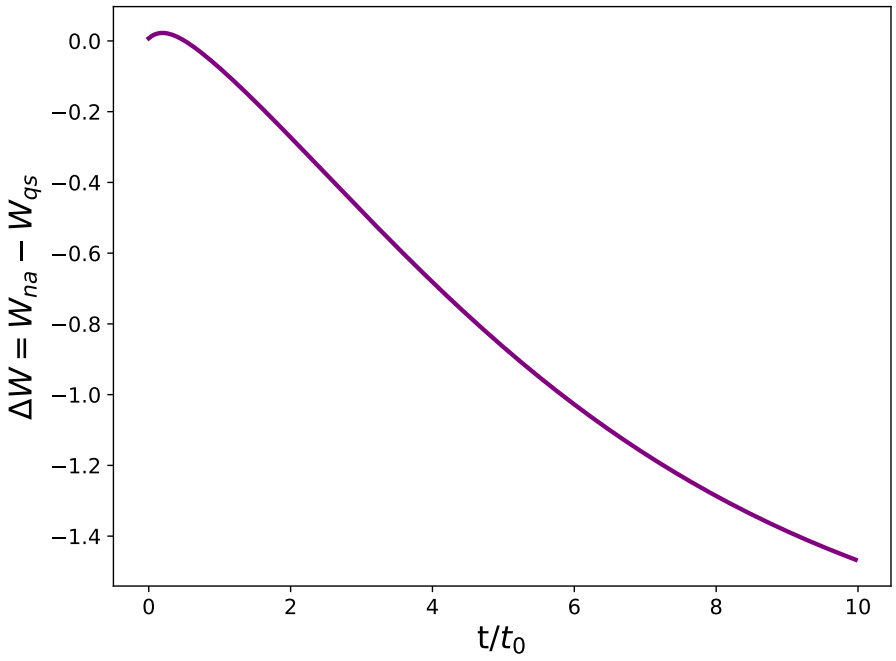

Figure 3.15 The difference in insertion work changes between the nonadiabatic and quasistatic cases

During the finite-time insertion, we observe the generation of quantum coherence from an initially incoherent thermal state. This is attributed to the non-adiabatic driving induced by the moving partition, which forces the system into a superposition of its instantaneous energy eigenstates. Subsequently, as the driving ceases, the coherence decays due to thermalization, as the system relaxes back to an equilibrium thermal state in the new potential via its coupling to the reservoir.

Following the position measurement, the system begins the expansion in a state of high coherence. While all coherence measures decay due to thermalization, their dynamics differ. Notably, the l_1 norm of coherence shows a more robust persistence midway through the expansion compared to other measures, particularly the custom C_w measure designed to probe low-energy coherence. This discrepancy suggests that the non-adiabatic dynamics transiently populate coherent superpositions between high-energy eigenstates. This effect, a signature of quantum friction, is most pronounced during the fastest portion of the expansion. The difference between the l_1 and C_w measures thus provides insight into the energy distribution of the generated coherence, isolating the contribution from these transient high-energy excitations.

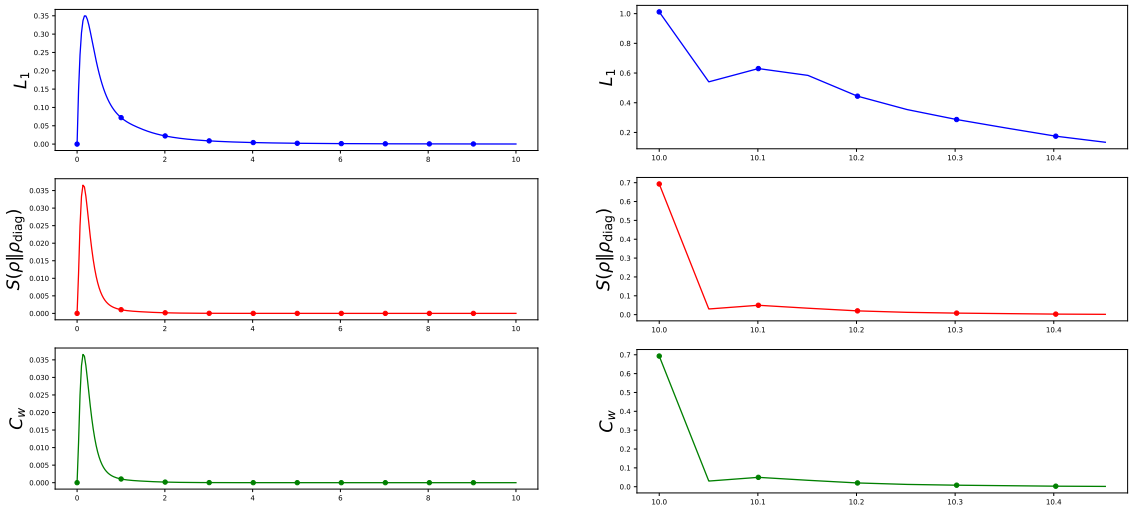

Figure 3.16 Comparison of coherence measures: (first column) insertion (quasistatic + finite-time), (second column) expansion (after measurement)

The simulation results for the finite-time expansion deviate significantly from the idealized, quasi-static Szilard engine model. The fact that the extracted work is less than the decrease in free energy, $W_{\text{actual}} < -\Delta F$, is direct evidence of dissipation. This irreversibility arises from the non-adiabatic nature of the expansion; rapid changes in the confining potential induce quantum transitions to excited states, a phenomenon known as quantum friction. Consequently, the ideal Szilard Information-to-Energy Transduction (SIST), where $W = k_B T \ln 2$, is not achieved. A portion of the energy is irrecoverably lost as heat, highlighting the fundamental trade-off between power and efficiency in finite-time quantum engines.

The final results of the changes in thermal quantities, obtained using Table 3.5, are given in Table 3.4.

Table 3.4 Thermodynamic quantities for each stage of the cycle

Quantity	**Insertion**	**Measurement**	**Expansion**	**Removal**	**Total**
ΔU	3.3896	0.0022	0.3465	-3.7382	0.0000
ΔF	-188.1925	47.0089	-50.1454	191.3290	0.0000
ΔS	2.8235	-0.6928	0.7441	-2.8748	0.0000
Total Work	0.6808	0.0000	-0.8892	0.0000	-0.2084
Total Heat	2.7088	0.0022	1.2356	-3.7382	0.2084

The standard well-defined temperature no longer works in the non-adiabatic regime. This occurs because different energy levels evolve at different rates during the insertion process, making it impossible to satisfy the Boltzmann condition $\frac{P_n}{P_m} =$

Table 3.5 Parameters for initial ground state scenario

n	**c**	γ_0	**T (K)**	η
18	1.15	0.07	300	0.05

$e^{-(E_n - E_{n+1})/k_B T}$ with a single, well-defined temperature T for all states in equilibrium. This breakdown from well-defined temperature emerges when the insertion time becomes shorter than the quantum speed limit $\tau < \hbar/\Delta E$, where ΔE represents the energy spacing of the system. The resulting non-equilibrium dynamics generate additional entropy production and irreversible work losses, as the populations cannot follow the changing potential. These effects play a crucial role in the finite-time quantum Szilard engine, where the discrete energy levels respond unevenly to the barrier insertion and the expansion. Since the quantum boundary layer thickness depends inversely on the square root of temperature in equilibrium, this emergent, ill-defined temperature prevents a direct quantification of shape-dependent boundary effects. As a result, finite-time operation introduces fundamental limitations on evaluating geometric contributions to the system's thermodynamics.

4. CONCLUSION

A finite-time quantum Szilard engine is investigated under size invariant shape transformation (SIST). We showed that different insertion speeds and temperatures control the thermodynamic parameters of the system. Although the insertion speed appears to be directly proportional to the work applied to the system during the insertion process, it behaves inversely with the work extracted during the expansion due to tunneling-related effects. The pseudo coherence measure C_w does not show significant differences when analyzed under varying insertion speeds. This is because the systems studied at different speeds do not undergo any shape deformation; the effect of insertion speed appears only in energy space, rather than in the spatial profile of the system. In the case of different temperatures, the shape effect becomes more pronounced in the C_w. This is because the thickness of the boundary layers is inversely proportional to temperature. The increase in boundary layer thickness enhances the effect of ground state reduction and leads to more prominent differences in the pseudo coherence measure C_w. Although coherence does not significantly influence work extraction in the system, it was shown to play a role in the states resulting from the SIST process.

To determine the optimal work extraction conditions, a geometric thermodynamic analysis is required. Additionally, further investigation is needed to perform the removal process more effectively and work extraction from the coherence. Effect of weak measurement also will be considered.

BIBLIOGRAPHY

Aharonov, Y., Albert, D. Z., & Vaidman, L. (1988). How the result of a measurement of a component of the spin of a spin-1/2 particle can turn out to be 100. *Phys. Rev. Lett.*, *60*, 1351–1354.

Aydin, A. (2020). *Quantum Shape Effects: A Theoretical Treatise on the Quantum-Mechanical Influence of Geometry in the Thermodynamics of Strongly Confined Nanostructures*. PhD thesis, Istanbul Technical University, Istanbul, Turkey. Energy Institute.

Aydin, A. (2023). Spectral properties of size-invariant shape transformation. *Physical Review E*, *107*(5), 054108.

Aydin, A. & Sisman, A. (2019). Quantum shape effects and novel thermodynamic behaviors at nanoscale. *Physics Letters A*, *383*(7), 655–665.

Aydin, A. & Sisman, A. (2023). Origin of the quantum shape effect. *Physical Review E*, *108*(2), 024105.

Aydin, A., Sisman, A., & Kosloff, R. (2020). Landauer's principle in a quantum szilard engine without maxwell's demon. *Entropy*, *22*(3), 294.

Baumgratz, T., Cramer, M., & Plenio, M. B. (2014). Quantifying coherence. *Physical review letters*, *113*(14), 140401.

Bennett, C. H. (1982). The thermodynamics of computation—a review. *International Journal of Theoretical Physics*, *21*(12), 905–940.

Boltzmann, L. (1877). *Über die Beziehung zwischen dem zweiten Hauptsatze des mechanischen Wärmetheorie und der Wahrscheinlichkeitsrechnung, respective den Sätzen über das Wärmegleichgewicht*. Kk Hof-und Staatsdruckerei.

Breuer, H.-P. & Petruccione, F. (2002). *The theory of open quantum systems*. OUP Oxford.

Brunelli, M., Genoni, M. G., Barbieri, M., & Paternostro, M. (2017). Detecting gaussian entanglement via extractable work. *Phys. Rev. A*, *96*, 062311.

Cai, C., Dong, H., & Sun, C. (2012). Multiparticle quantum szilard engine with optimal cycles assisted by a maxwell's demon. *Physical Review E—Statistical, Nonlinear, and Soft Matter Physics*, *85*(3), 031114.

Čápek, V. & Sheehan, D. P. (2005). *Challenges to the second law of thermodynamics: theory and experiment*. Springer.

Cuzminschi, M., Zubarev, A., Iordache, S.-M., & Isar, A. (2023). Influence of the seed of measurement on the work extracted in a quantum szilard engine. *iScience*, *26*(12).

Das, D., Thomas, G., & Jordan, A. N. (2023). Quantum stirling heat engine operating in finite time. *Physical Review A*, *108*(1), 012220.

Davies, P., Thomas, L., & Zahariade, G. (2021). The harmonic quantum szilárd engine. *American Journal of Physics*, *89*(12), 1123–1131.

Elouard, C., Herrera-Martí, D., Huard, B., & Auffeves, A. (2017). Extracting work from quantum measurement in maxwell's demon engines. *Physical Review Letters*, *118*(26), 260603.

Erdman, P. A., Czupryniak, R., Bhandari, B., Jordan, A. N., Noé, F., Eisert, J., & Guarnieri, G. (2025). Artificially intelligent maxwell's demon for optimal control of open quantum systems. *Quantum Science and Technology*, *10*(2), 025047.

Firat, C. & Sisman, A. (2009). Universality of the quantum boundary layer for a maxwellian gas. *Physica Scripta*, *79*(6), 065002.

Gemmer, J. & Anders, J. (2015). From single-shot towards general work extraction in a quantum thermodynamic framework. *New Journal of Physics*, *17*(8), 085006.

Gibbs, J. W. (1878). On the equilibrium of heterogeneous substances. *American journal of science*, *3*(96), 441–458.

Jacobs, K. (2014). *Quantum measurement theory and its applications*. Cambridge University Press.

Kammerlander, P. & Anders, J. (2016). Coherence and measurement in quantum thermodynamics. *Scientific reports*, *6*(1), 22174.

Kim, S. W., Sagawa, T., De Liberato, S., & Ueda, M. (2011). Quantum szilard engine. *Physical review letters*, *106*(7), 070401.

Kosloff, R. (2013). Quantum thermodynamics: A dynamical viewpoint. *Entropy*, *15*(6), 2100–2128.

Landauer, R. (1982). Uncertainty principle and minimal energy dissipation in the computer. *International Journal of Theoretical Physics*, *21*(3), 283–297.

Lloyd, S. (1997). Quantum-mechanical maxwell's demon. *Physical Review A*, *56*(5), 3374.

Pastor, G. (2019). *Introduction to Statistical Physics*. Kassel, Germany: Universität Kassel, Institut für Theoretische Physik. pp. 126–128.

Peterson, J. P., Sarthour, R. S., & Laflamme, R. (2020). Implementation of a quantum engine fuelled by information. *arXiv preprint arXiv:2006.10136*.

Planck, M. (1978). Über das gesetz der energieverteilung im normalspektrum. In *Von Kirchhoff bis Planck: Theorie der Wärmestrahlung in historisch-kritischer Darstellung* (pp. 178–191). Springer.

Plenio, M. B. & Vitelli, V. (2001). The physics of forgetting: Landauer's erasure principle and information theory. *Contemporary physics*, *42*(1), 25–60.

Sagawa, T. (2012a). Thermodynamics of information processing in small systems. *Progress of theoretical physics*, *127*(1), 1–56.

Sagawa, T. (2012b). Thermodynamics of information processing in small systems. *Progress of theoretical physics*, *127*(1), 1–56.

Shannon, C. E. (1948). A mathematical theory of communication. *The Bell system technical journal*, *27*(3), 379–423.

Sisman, A., Ozturk, Z. F., & Firat, C. (2007). Quantum boundary layer: a non-uniform density distribution of an ideal gas in thermodynamic equilibrium. *Physics Letters A*, *362*(1), 16–20.

Szilard, L. (1929). Über die entropieverminderung in einem thermodynamischen system bei eingriffen intelligenter wesen. *Zeitschrift für Physik*, *53*(11), 840–856.

Van Vu, T. & Saito, K. (2022). Finite-time quantum landauer principle and quantum coherence. *Physical review letters*, *128*(1), 010602.

Vinjanampathy, S. & Anders, J. (2016). Quantum thermodynamics. *Contemporary Physics*, *57*(4), 545–579.

Violaris, M. & Marletto, C. (2022). The irreversibility cost of purifying szilard's engine: Is it possible to perform erasure using the quantum homogenizer? *arXiv preprint arXiv:2205.11310*.

Von Neumann, J. (2013). *Mathematische grundlagen der quantenmechanik*, volume 38. Springer-Verlag.

Yadin, B., Ma, J., Girolami, D., Gu, M., & Vedral, V. (2016). Quantum processes which do not use coherence. *Physical Review X*, *6*(4), 041028.

Zhou, T.-J., Ma, Y.-H., & Sun, C. (2024). Finite-time optimization of a quantum szilard heat engine. *Physical Review Research*, *6*(4), 043001.

Zurek, W. H. (1984). Maxwell's demon, szilard's engine and quantum measurements. In *Frontiers of nonequilibrium statistical physics* (pp. 151–161). Springer.